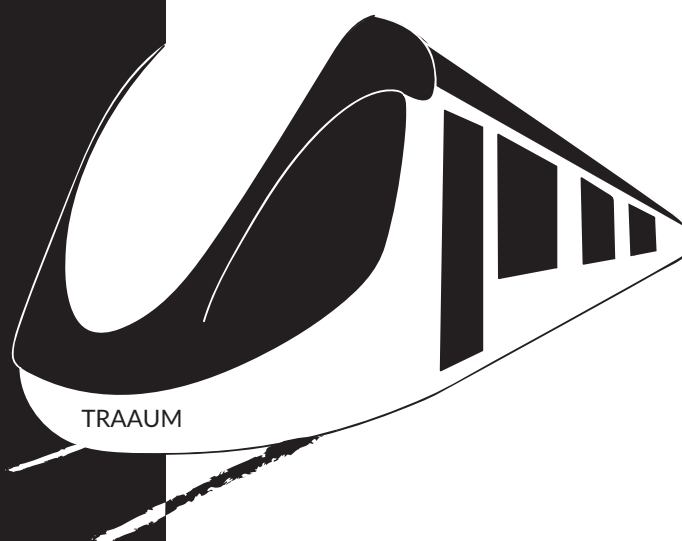


Optimal control of energy storage systems with power converters

- A catenary free tram case study



Master thesis

by

Endika Delgado Del Dujo

Group number: 15gr1037

June 2015



AALBORG UNIVERSITET



Electronics and IT
Aalborg University
<http://www.aau.dk>

AALBORG UNIVERSITY
STUDENT REPORT

Title:

Optimal control of energy storage systems with power converters

Theme:

Control and Automation

Project Period:

Spring Semester 2015

Project Group:

15gr1037

Participant(s):

Endika Delgado Del Dujo

Supervisor(s):

John Leth
Jan Dimon Bendtsen

Copies: 4

Page Numbers: 83

Date of Completion:

June 3, 2015

Abstract:

The present document covers the modeling and control of a tram that runs free of overhead lines, and draws the power from a battery pack. The goal of this work is to derive two control strategies, that can then be compared. The first strategy is closer to the conservative approach taken by the industry. The second one, is what is known as Model Predictive Control. The thesis covers the modeling of the tram first, and then the design of the controllers. The conservative strategy includes a series of linear controllers and makes use of EKF as estimators. Simulation results are shown. The MPC strategy is covered and setup. However, no results are shown.

The content of this report is freely available, but publication (with reference) may only be pursued due to agreement with the author.

Contents

| | |
|--|------------|
| Preface | vii |
| 1 Introduction | 1 |
| 1.1 Structure of this work | 2 |
| 1.2 Methods | 3 |
| 2 Modeling | 5 |
| 2.1 Introduction | 5 |
| 2.2 Battery model | 7 |
| 2.2.1 Single cell models | 7 |
| 2.2.2 Battery pack | 10 |
| 2.2.3 Model | 11 |
| 2.3 Power electronic converters | 11 |
| 2.3.1 Boost converter example | 14 |
| 2.4 Interleaved boost converter | 19 |
| 2.4.1 Switched model | 19 |
| 2.4.2 Generalized average model | 21 |
| 2.4.3 Switched model vs. GAM | 27 |
| 2.5 SVM Inverter | 28 |
| 2.6 Induction Machine | 32 |
| 2.6.1 Three phase model equations | 33 |
| 2.6.2 2-phase model | 34 |
| 2.7 Field Oriented Model | 36 |
| 2.7.1 Moving reference frame | 38 |
| 2.7.2 Field Oriented Control | 40 |
| 3 Control objectives and design | 43 |
| 3.1 Controller design: Industry Approach | 43 |
| 3.2 Battery state estimation | 44 |
| 3.2.1 Linear model and estimation | 45 |
| 3.2.2 EKF and parameter estimation | 46 |

| | | |
|----------|--|-----------|
| 3.2.3 | Simulation results of the estimator | 49 |
| 3.2.4 | Interleaved DC-DC converter | 51 |
| 3.2.5 | Simulation results | 53 |
| 3.2.6 | Induction Machine | 54 |
| 3.2.7 | Indirect Field Oriented Control | 56 |
| 3.2.8 | State estimation | 59 |
| 3.2.9 | Simulation results of the observer based controller of the motor | 62 |
| 3.2.10 | Performance of the classical control approach | 63 |
| 4 | Model Predictive Control | 67 |
| 4.1 | Model Predictive Control Approach | 67 |
| 4.2 | MPC model | 69 |
| 4.3 | State and input constraints | 72 |
| 4.3.1 | Constraints imposed by the battery | 72 |
| 4.3.2 | Contraints imposed by the DC-DC converter | 73 |
| 4.3.3 | Constraints imposed by the induction motor | 73 |
| 4.3.4 | Summary of the constraitns | 75 |
| 4.3.5 | Objective function | 76 |
| 4.3.6 | Reference tracking | 77 |
| 4.4 | Conclusion | 78 |
| 5 | Conclusion | 79 |
| | Bibliography | 81 |

Preface

This work is presented as the Master Thesis for the completion of a MsC. Control & Automation.

Aalborg University, June 3, 2015

Endika Delgado Del Dujo
<edelga13@student.aau.dk>

Chapter 1

Introduction

The demand for greener standards of living and production in today's world has steered the world's different industries towards the development of more efficient systems without compromising in quality and/or reliability. One of the outcomes of such a philosophy is the further development of energy storage systems. These systems include an energy storage device, usually batteries or ultracapacitors, and a power converter, often a DC-AC converter. The tandem load-converter-battery is more and more commonplace, and the electric car is probably its maximum exponent. It can also be found in trams and metros, where an energy storage system is used to recover energy from the braking, but it also may allow for running without catenary between stops. An example of these are Taiwan's and Seville's trams, developed by CAF P&A. Even elevators are starting to incorporate energy storage systems, such as the Zero Energy Lift concept of Orona, where an elevator may run only on some initial charge of a battery, consuming from the grid just enough to compensate for the losses in the system.

Not only in transportation this tandem finds purpose. With the growth of renewable energies, and its spread to domestic level, the electrical grid becomes more and more populated with stochastic energy sources. The user's goal for installing these technologies in the household may well be zero balance in their energy bill or even profit. Regardless the case, an energy storage system is required for maximum benefit. Panasonic's E3/DC can be taken as an example.

To meet the efficiency goals, when designing the controller, the dynamics of the load, the battery and the converter must be under constant consideration.

Batteries are restrictive components that impose some constraints in the way they can deliver power, both in time and value. Furthermore, the load's performance demands must be met. The problem is to bring both systems to terms, meeting the performance goals without straining the energy storage system beyond its limits,

minimizing losses, and prolonging its useful life. Finally, converters are non-linear devices whose controllers are usually developed to work optimally around different working points, however more sophisticated strategies can be investigated.

The aim of the thesis is to cover the different topics inside these type of systems, which can be summarized as follows:

- Modeling of batteries, converters and typical loads such as AC motors, etc.
- Estimation of the load and state of charge of the battery
- Control of power converters

Because the topic is wide, and it would be impossible to consider all the technologies and possibilities. A catenary free tram has been chosen as case study. The reason for choosing this system is that it allows for modelling of power converters, battery packs and a load. Another peculiarity of this system is that all technologies considered are mature, however the industry keeps approaching control in a very conservative manner. As a matter of fact, to use as a base to compare the control developed in this thesis, a control strategy that resembles that of the industry has been considered.

1.1 Structure of this work

This work is divided in five chapters, including this introduction. Chapter 2 covers the modeling of the system. It starts by describing the system, and continues with an introduction to batteries. It follows by describing the basics about power converters, and induction motors. At the end the sections dedicated to each subsystem the models produced are presented along with some simulation results. Chapter 3 covers the design of a controller that resembles those used in the industry. The scheme is based on controlling the individual subsystems such that their individual effort allows for the system to achieve an adequate performance. The controllers employed are linear. The section starts by covering the battery state of charge estimator, and some results on online parameter estimation of the battery are shown. It follows by describing the design of a cascaded loop for the DC-DC converter. The idea is current can be controlled individually under the assumption that its dynamics are faster than those attach to the voltage. This will serve as the inner loop. An outer loop is then used to control the current, where the manipulated variable is the current reference for the inner loop. The chapter follows with the design of a speed and current control for the induction motor. Some of the practices show in the literature and used, and a controller is designed. Furthermore, a Kalman filter is used for estimation of the flux and angle of the rotor flux. This is certainly the most interesting part of this chapter, as it employs a non-linear coordinate transformations, and clever use of reference frames to attain control of the system. The chapter concludes with an

analysis of the control system as a whole. Chapter 4 cover the development of Model Predictive Control for the system. Due to the computationally intensive nature of the approach, low sampling frequencies are imposed. Therefore, the current loops developed in Chapter 3 for the DC-DC converter and induction machine are employed. The task of the MPC is then to compute the optimal references for this loops, based on the energy stored in the capacitor and the battery. Hence, MPC developed is an holistic approach to the control of the system. The chapter starts by posing the reciding horizon problem. The next section covers the creation a linear model that captures the system behavior. The system needs to resembles the actual system, but not so convoluted that imposes unrealistic computational requirements. The chapter continues by covering the constraints. This are obtained from the system spectifications, but also dynamics. Finally reference tracking in Model Predicted Control is introduced. Unfortunately, no results can be shown for MPC. The thesis closes with Chapter 5, where the results of the thesis are discussed.

Yet a last remark. A very relevant conclusion is obtained at the end of 4, if not of the technical type, but that should be clear for anyone working in the field, or for the same, any field.

1.2 Methods

All the models derived in this project have been derived from first principle analysis. Furthermore, the value of the parameters in the system can be easily found in the literature and industrial suppliers when applies.

Because of the dimension of the system under consideration, only simulation results are shown. It must be said however, that with exception of the battery, the simulation models used in the thesis are quite accurate. This is because all the systems covered, again saving the battery, are very deterministic and the parameter can be usually easily determined or even directly measured.

It should mentioned as well that this is a prospective work, with no real life application considered, despite that pragmatism has been main philosophy during most of the development of this work. Despite the ideal aim of this text, application can easily be found for all the theory covered here.

Chapter 2

Modeling

2.1 Introduction

This chapter covers the modeling of the system. The system at hand is the whole traction set of tram, this includes:

- A battery pack that works as a power source
- A DC-DC converter that regulates the rate at which power is drawn from the battery
- An DC-AC converter that serves as actuation for an induction Motor
- An induction motor

For a single tram, more than one set exists. As a matter of fact a typical configuration would be the one shown in figure 2.1. In the figure above a tram with two traction

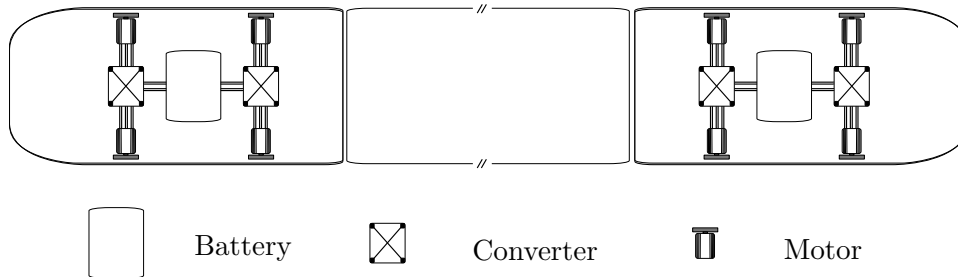


Figure 2.1: Top view of the tram with two traction cars. Each battery is connected to two inverters, that are in turn connected to two motors.

cars is shown. Each traction car features a battery pack, two traction converters with two motors per traction converter. In an effort to simplify the model, while retaining all the important features, some assumptions have been made:

- There is no slip on the wheels
- There are no mechanical brakes
- The mechanical load is shared equally among the eight motors of the system
- As a consequence, a single motor is modeled for an inverter with halved power rating
- In the same manner, the battery is downsized to a fourth of its actual size

The first assumption has implication in the mechanical model. Since it is not the focus of this work to model the tram to detail, it can be safely disregarded. The second assumption has bigger impact however. By removing the possibility of a mechanical brake, the tram relies exclusively on the motor to stop movement. Of course, in a real applications mechanical brakes exist. The consequence is a higher reliance on the motor speed control, but also bigger return of energy to the battery during braking, hence, higher. The third assumption is a simplification of the actual system. Differences in the motor mechanical loads may happen for many reasons: different friction coefficients, unbalanced share of mass inside the car, speed differences between the motors in the inside of the curve and outside, etc. Because it is impossible to account for all the situations in the time allocated for this work, the decision to assume equal load sharing has been made. The following assumption is a consequence of the third assumption. Finally, the fifth assumption, is yet again another simplification of the actual system. The deviation from reality resides in that during real life operation, the different loading of the motors connected to a single battery pack will impact the inner state of the battery, while in the considered model, the battery state depends exclusively on the actions of the motor considered.

The model presented in this chapter is summarized in figure 2.2. Each model output is an input for the two contiguous systems. Thus the battery model computes the voltage of the battery at every instant. The DCDC converter model uses the motor's current and battery voltage to compute the battery current and bus voltage. Finally the induction motor's model compute the bus current and torque from the speed of the load and the bus voltage.

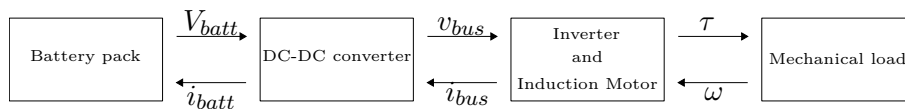


Figure 2.2: Top view of the tram with two traction cars. Each battery is connected to two inverters, that are in turn connected to two motors.

The chapters starts by describing the battery pack model in section 2.2. It starts introducing how batteries work, followed by a brief description of the different

modeling approaches in the literature. The section ends with a model of the battery pack. In section 2.3 the basic theory about power electronic converters is laid down. This is used to later develop a switched model, as well as a Generalized Average Model, for the DC-DC converter in section 2.4. Furthermore, section 2.5 describes the inverter and Space Vector Modulation. Finally, section 2.6 covers the model of the induction motor. The two phase induction model that is used for simulation is covered. A model that can be used for control design, known as field oriented model, is then derived upon the two phase model. Furthermore, the transformation from and to the different frames in which the motor is represented are covered.

2.2 Battery model

Batteries are electrochemical devices that store electrical energy. When electric voltage is applied to the batteries and a current starts to flow into them a series of chemical reactions occur that store the energy as an electrical potential, or voltage, between the two electrodes. The process by which this happens strongly depends on the chemistry. During this work only Li-ion batteries are considered. Non-rechargeable batteries are usually known as primary batteries, while rechargeable are known as secondary batteries. From now on, for the sake of brevity, the term battery will be used univocally for secondary batteries.

The smallest working unit inside a battery is the cell. In many cases, specially in portable electronics and small toys, the battery consists of a single cell. In bigger appliances, industrial equipment and vehicles a battery consists of many cells connected in series and parallel. These are usually referred to as battery packs. Sometimes, when talking about battery packs, the term may also include the helper electronics that keep the internal cells balanced, control the cooling and provide information about the state of the battery. This is known as Battery Management System (BMS). In the sequel when referring to the battery pack, the BMS is not accounted for unless explicitly stated.

What follows is a series of explanations on the concepts needed for modeling the battery pack. At the end of the section the model is described.

2.2.1 Single cell models

Battery models are presented in the literature mostly as single cell models. There exist essentially two types of approaches to model batteries: electrochemical models and electrical equivalent models. Electrochemical models try to model the chemical reactions inside a cell using the Butler-Volmer equation for electrochemical kinetics [26][29]. These models are obviously very dependent on the chemistry of the cell. On

top of that, they make use of a high number of parameters and are very complex, which makes them not practical for the use in this work. Electrical equivalent models try to capture the electrical behavior of the cell by means of an equivalent circuit, most usually consisting on an RC network and some numerical, experiment based, approximations of the insides of the cell [19][31][22]. Because of its simplicity, yet accurate simulation value, this is the approach chosen for this work.

Equivalent circuit

An electrical circuit is used to capture the dynamic electrical behavior of the cell. The circuit consists on at least one RC network connected in series to a variable voltage source, known as open circuit voltage (OCV). How the OCV is modeled will be treated later. The series impedances (RC networks) in the circuit are often

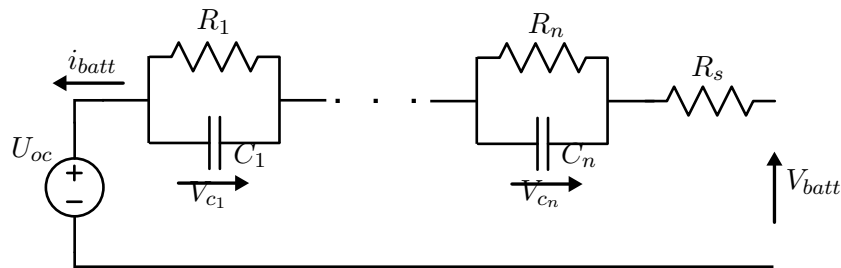


Figure 2.3: Model of a battery cell

given some physical meaning in the literature [18][17], as it may be the electrolyte's resistance, ion diffusion, polarization, etc. Other approach is just looking at the cell from a purely behavioral perspective, and set the time constants of the circuitry based on experiments, as in [24][15]. Time constants are determined from experimentation, by exciting the batteries within some specific bandwidth of interest. Additionally, the impedance is often made dependent of the state of charge [24][31][18]. The OCV and SoC are explained in the sequel.

State of charge and open circuit voltage

State of Charge (SoC) and Open Circuit Voltage (OCV) concepts are strongly related. State of charge is often stated as the amount of energy stored in the battery. However most of the time it is computed as the amounts of coulombs or Ah (Ampere-hour) in the battery:

$$\text{SoC} = \text{SoC}(0) + \int_0^t \frac{i}{C} dt \quad (2.1)$$

where:

| | | |
|-----|--------------------------------|---------|
| i | is the battery current | [A] |
| C | is the capacity of the battery | [A · s] |

Indeed, the SoC, when computed as (2.1), it is hardly a measure of energy, as Ah or As (Ampere-second) are not equivalent to Jules or Watt-hours. However it is still a valid metric, and it is in fact a very reliable indicator of energy. In (2.1) the value of SoC will takes values from 0 to 1, instead of the usual 0% to 100%.

Open circuit voltage is the driving voltage in the battery. This is the voltage generated by the chemical reactions, and it is very dependent on the SoC. This is the reason it is also sometimes used to determined the SoC of the battery, instead of current integration. The profile and behavior of this voltage depends very much on the chemistry of the battery. In this work the focus is on Li-ion batteries, and the OCV behavior for other chemistries is of no consequence to it. The main characteristics of the Li-ion batteries' SoC-OCV profiles is its flatness, making it difficult to be used as SoC indicator. Additionally, Li-ion batteries present hysteresis in the OCV [19]. In [19] the model of the hysteresis is purely data driven. The OCV is

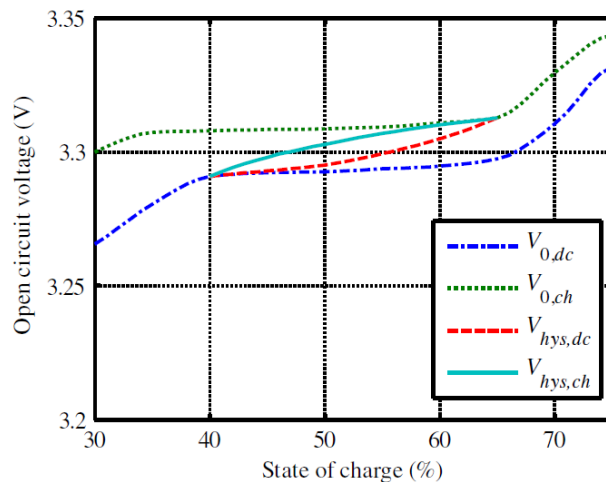


Figure 2.4: Hysteresis phenomena during charge and discharge of li-ion battery [4]

mapped for different values of SoC and computed at each instant. Similarly, in [4], a polynomial approximation is used. In [17], hysteresis is approximated using the following equation:

$$\dot{V}_h = -\frac{1}{\beta}i(\text{sign}(i)V_h - V_{h_{max}}) \quad (2.2)$$

$$V_{oc} = U_{oc} + V_h \quad (2.3)$$

where:

| | | |
|---------------|--|---------|
| $V_{h_{max}}$ | is the maximum deviation from the mean VOC due to the hysteresis | [V] |
| V_h | is the deviation from the mean VOC due to hysteresis | [V] |
| U_{oc} | is the mean value of the VOC | [V] |
| β | is a constant obtained empirically | [A · s] |

The resulting behavior can be seen in figure 2.5. In equation (2.2), V_h , cannot take

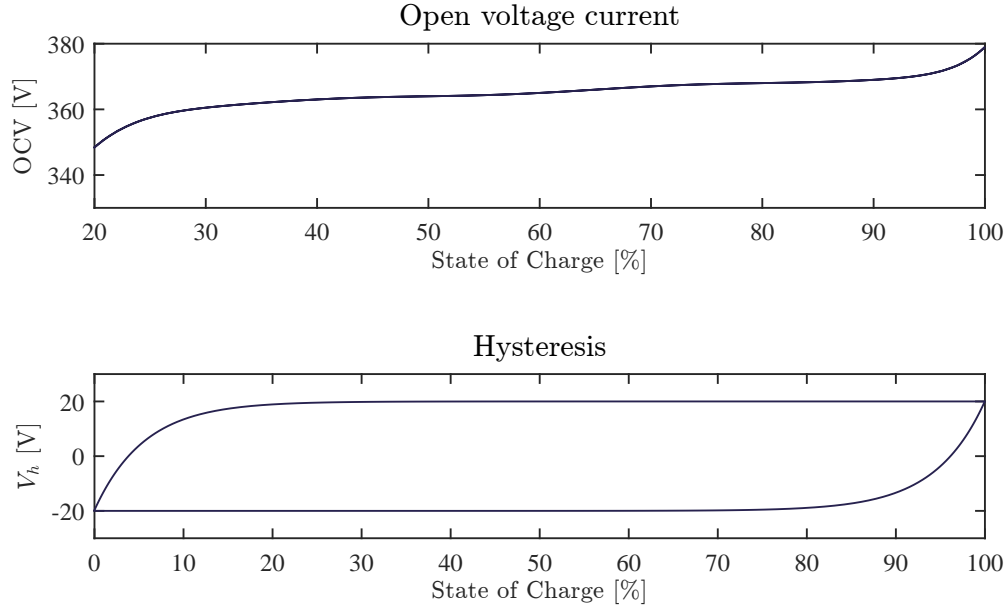


Figure 2.5: Open circuit voltage and hysteresis as model by the equations presented

values bigger or smaller than $\pm V_{h_{max}}$. Notice that when V_h reaches the value $V_{h_{max}}$ when charging ($i > 0$), its derivative is zero. Same effect when discharging. This limitation is therefore symmetric, which fits the behavior shown in [19]. The term $\frac{1}{\beta}i$ relates the dynamics of the hysteresis to the current. This is the chosen method to model the hysteresis, as it doesn't require extensive data and long experiments. Finally, the mean voltage U_{oc} is modeled by means of a nth order polynomial fitted from data.

2.2.2 Battery pack

Batteries consists of several cells connected in series and parallel to attain the energy and voltage goals of the system. As opposed to the cell models, it is relatively difficult to find models for battery packs in the literature. In some cases, a model for a single cell is developed under the assumption that the battery pack can be modeled by stacking several cell models [17][24]. For small packs this is doable, but for a big

system it's not convenient because of the computational load. A different approach consists on considering the pack as a single battery, producing a model similar to the single cell model, but accounting for the phenomena due to the difference between cells [18]. Finally, in [15] it is proposed to model the battery pack itself under the assumption that it is well designed. That is, cells don't present big variations and inside the pack no big temperature gaps exist. This is the approach taken, as it is assumed that the battery pack has already being designed with purpose. Additionally, it doesn't require a characterization of how the cell parameters distribute as in [24] and [18].

2.2.3 Model

The model is summarized now. Equations for the RC network and SoC are linear:

$$\begin{bmatrix} \dot{V}_{c_1} \\ \dot{V}_{c_2} \\ \vdots \\ \dot{V}_{c_n} \\ \text{SoC} \end{bmatrix} = \begin{bmatrix} -\frac{1}{R_1 C_1} & 0 & \dots & 0 \\ 0 & -\frac{1}{R_2 C_2} & 0 & \dots & 0 \\ \vdots & & \ddots & & \vdots \\ 0 & \dots & & -\frac{1}{R_n C_n} & 0 \\ 0 & \dots & & 0 & 0 \end{bmatrix} \cdot \begin{bmatrix} V_{c_1} \\ V_{c_2} \\ \vdots \\ V_{c_n} \\ \text{SoC} \end{bmatrix} + \begin{bmatrix} \frac{1}{C_1} \\ \frac{1}{C_2} \\ \vdots \\ \frac{1}{C_n} \\ \frac{1}{C} \end{bmatrix} \cdot i \quad (2.4)$$

The equations describing OCV behavior are:

$$U_{OC} = \sum_{k=0}^n a_k \cdot \text{SoC}(t)^k \quad (2.5)$$

$$\dot{V}_h = -\frac{1}{\beta} i (V_{h_{max}} + \text{sign}(i)V_h) \quad (2.6)$$

$$V_{oc} = U_{OC} + V_h \quad (2.7)$$

Finally the output voltage of the battery is:

$$V_{batt} = \sum_n V_{c_n} + V_{oc} \quad (2.8)$$

Before concluding this section, a simulation of the battery model subjected to an arbitrary train of pulses is shown in figure 2.6.

2.3 Power electronic converters

Power electronic converters, power converters, or simply, converters, are electronic systems that use high power versions of common semiconductors, like bipolar transistors, MOSFETS, diodes, or specialized ones like IGBTs or thyristors, to "shape" electrical energy. Different converter topologies can achieve different purposes like

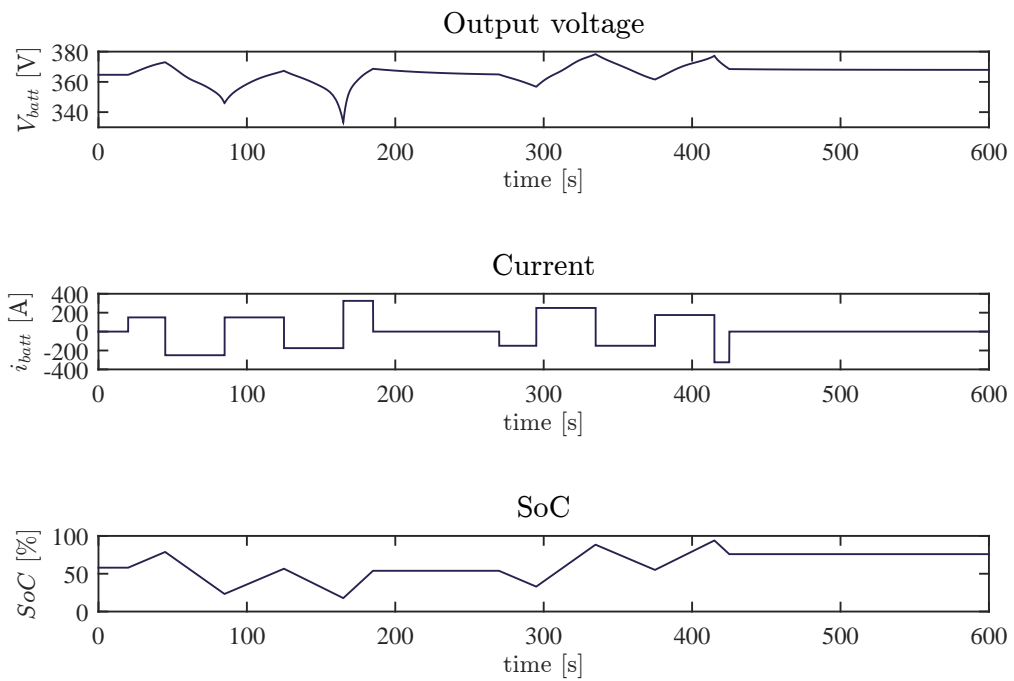


Figure 2.6: Voltage, battery current, and state of charge of the battery when subjected to a train of current pulses

- Rectification: converting an AC voltage or current into DC.
- Amplification
- Inversion: converting an AC voltage or current into DC

This section covers the modeling of power converters for simulation but it also gives hints on the mathematical modeling of the converters for control purposes. Some references to understand power electronics converters are [20][2]. They cover power converters from the design point of view, including the basic topologies. However they give good insight on the necessary concepts and help understanding the behavior of any type of converter, and therefore they are very useful for modeling. [27] covers modeling of the converters and most usual control techniques, and it even goes into non-linear control of converters. Finally, [28] make some interesting points from the mathematical perspective when it comes to modeling of control converters, treating them as switched systems. It also includes a chapter on simulation, where it addresses the difficulties and options when simulating power electronic converters.

The purpose of this section is to show the modeling of both the inverter and an interleaved dc-dc power converter. During the modeling, some assumptions have been made:

- Switches are ideal. This implies:
 - Switching is instantaneous. That is there is no continuous transition from open to close or vice versa
 - When open, resistance is infinity. When close resistance is zero
- Switching frequency is constant. This true for most of the practical converters as well.

Instantaneous switching is a fair assumption, with an important implication. Switching from an open state to a close state, and vice versa, happens in a few microseconds, or even nanoseconds. This indeed mean that their effect on the dynamics is negligible. However, when the switch closes, voltage accross the switch decays while current rises, and the opposite when it open. This transition translates into switching losses, and by considering instant transitions, they will not be accounted for in the model. There is a powerful reason not include them, and is that they are difficult to model accurately, and because of the fast transition, it would slow simulation even further. Furthermore, even though this losses are big in absolute terms, they are not so big in relative terms, reaching some converters efficiencies of 99%.

Modeling of power converters will first be addressed with a simple example. Then the inverter and the interleaved dc-dc converter will be addressed.

2.3.1 Boost converter example

In the literature, one can find many examples where a buck converter is used to cover the basics on power converters [20][28]. The reason to choose the slightly more complicated boost converter to explain power converters is that it shows the important role of the inductance in many topologies. The converter in (2.7) is the classical boost

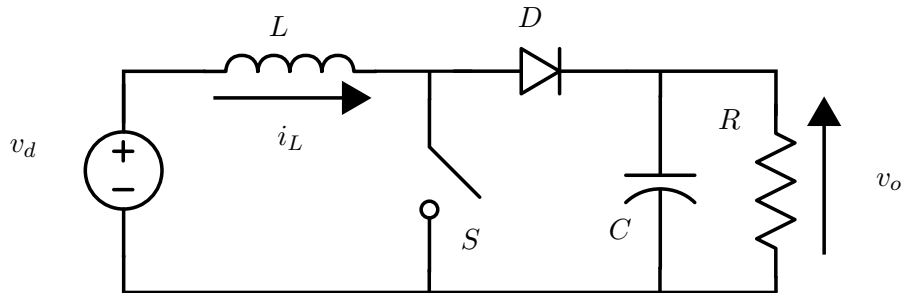


Figure 2.7: Boost converter

converter. The boost converter is also known as step-up converter, as it transforms a dc electrical voltage into a another dc voltage of higher value. In practice, the boost converter is not implemented as shown in the figure, however it serves its didactic purpose the same.

The boost converter works as follows. First consider that there is a voltage v_o across capacitor C , bigger than voltage v_d and switch S is open. Some current i_L is flowing through L . When the switch S is closed, a current i_L starts flowing through the inductance L . Notice that when the switch S is closed, the voltage across it is zero. This results in the circuit equivalent shown in figure 2.8. The converter can

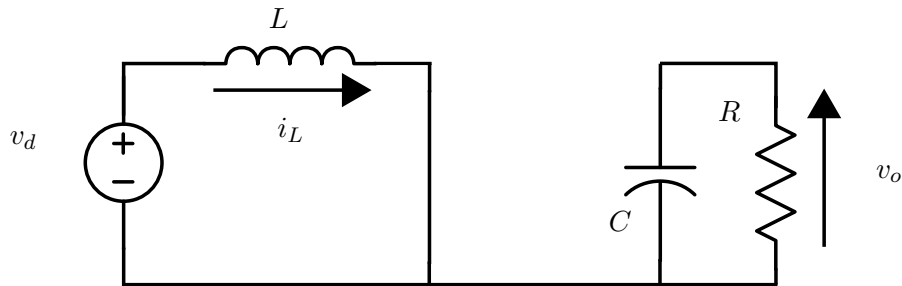


Figure 2.8: Mode 1: The diode separates the converter into two circuits

be modeled as two separated circuits. One with the inductor and the source, the other including the capacitor and the resistance. This separation is due to the diode D , which blocks any current flowing from the capacitor through the switch. This results in a current of increasing value that flows through inductor L , while capacitor

C discharges through R:

$$\frac{di_L}{dt} = \frac{v_d}{L} \quad (2.9)$$

$$\frac{dv_o}{dt} = -\frac{v_o}{RC} \quad (2.10)$$

When the switch S opens again, current stops flowing through it. The current i_L don't have any other path that is not through D and into C and R, effectively charging C and increasing its voltage, and therefore output voltage. This can be shown again as an equivalent circuit in figure 2.9.

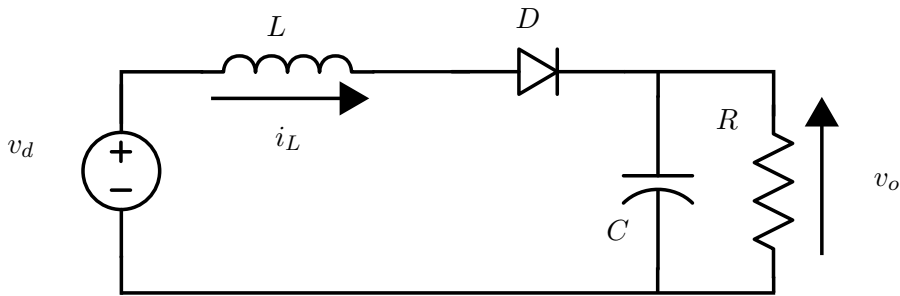


Figure 2.9: Mode 2: Current goes through the diode and into the load

The resulting equations are

$$\frac{di_L}{dt} = \frac{v_d - v_o}{L} \quad (2.11)$$

$$\frac{dv_o}{dt} = \frac{1}{C} \left(i_L - \frac{v_o}{R} \right) \quad (2.12)$$

Under the initial assumption that $v_o > v_d$, the current i_L starts decreasing in value. Figure 2.10 summarizes this behavior.

From this equations one can deduce the important role the inductance plays in the converter. When the switch opens, the inductance forces the current to keep flowing, effectively adding its own voltage to the input voltage v_d . By controlling the time the switch is on and off, one can control the input-output voltage ratio. As a matter of fact, the steady state ratio depends only on this. This can be shown using equations (2.9) and (2.11). During steady-state, the mean value of i_L doesn't change, and assuming a big enough capacitor C, the drop in the output voltage during the off period is negligible. This implies that during the off ($S = 0$) period, i_L decreases as much as it increased during the on ($S = 1$) period. Or in other words, the area under v_L in figure 2.10 during the on period is the same as during the off period:

$$v_d \cdot t_{on} = -(v_d - v_o) \cdot t_{off} \quad (2.13)$$

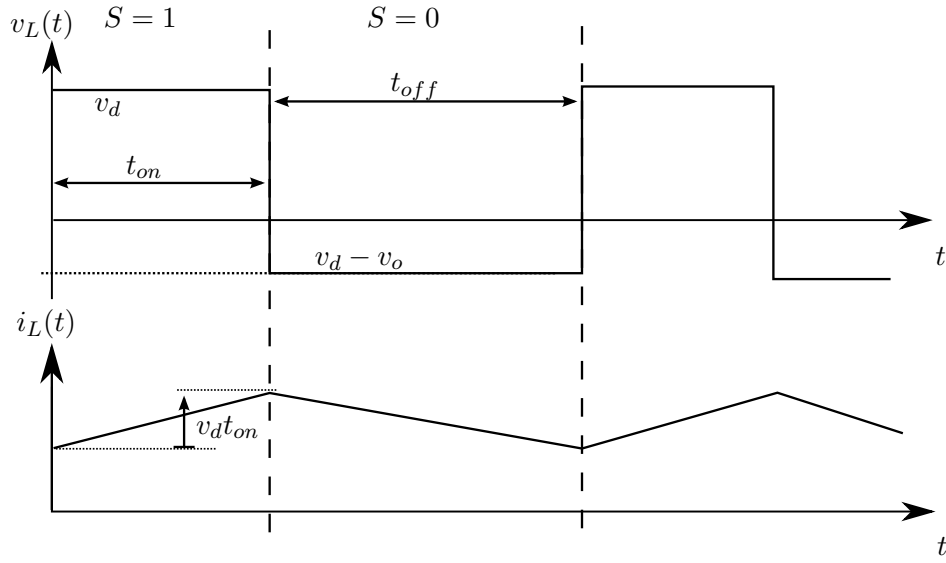


Figure 2.10: Current and voltage in a boost converter during steady-state operation

Dividing both sides by the switching period $T_{sw} = \frac{1}{F_{sw}}$, and introducing a term δ , known as duty ratio:

$$\frac{t_{on} + t_{off}}{T_{sw}} = 1 \quad (2.14)$$

$$\frac{t_{on}}{T_{sw}} = \delta \quad (2.15)$$

$$\frac{t_{off}}{T_{sw}} = 1 - \delta \quad (2.16)$$

$$V_d \cdot \delta = -(V_d - V_o) \cdot (1 - \delta) \quad (2.17)$$

$$\frac{V_o}{V_d} = \frac{1}{1 - \delta} \quad (2.18)$$

When the converter behaves like this, it is known as continuous-mode operation or continuous conduction mode. However it may happen that the current i_L drops to zero while the switch is off and before it turns on again.

This may easily happen when the load is too big, and therefore the current decreases faster. When this happens, it is known as discontinuous-mode operation or discontinuous conduction mode. The existence of a discontinuous mode is common in converters that include a fly-wheeling diode. During discontinuous mode the circuit looks like figure 2.12. And the resulting equations are:

$$\frac{di_L}{dt} = 0 \quad (2.19)$$

$$\frac{dv_o}{dt} = -\frac{V_o}{RC} \quad (2.20)$$

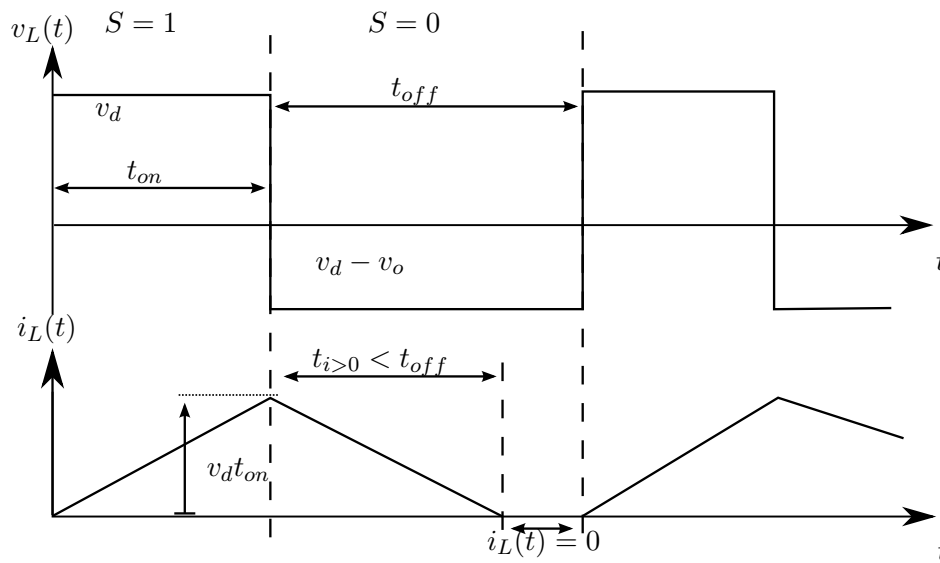


Figure 2.11: The boost converter going into discontinuous mode operation. The current drops to zero before the end of the switching period

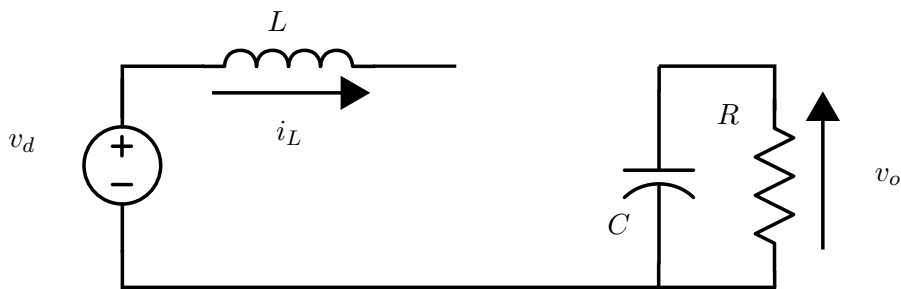


Figure 2.12: Mode 3: Discontinuous conduction mode

From the explanation given so far, one may deduce that power converters can be modeled indeed as switched linear systems. A set of linear models describe the different modes of operation, and a selection function decides the model at each instant. That is

$$\dot{x}(t) = \sum_{i=1}^m q_i(t, x(t)) (A_i x(t) + B_i u(t)) \tag{2.21}$$

where:

- A_i is the A matrix of mode i
- B_i is the B matrix of mode i
- q_i is a selection function that may only take values 0 or 1
- x is the state vector
- u is the input vector

If there is no discontinuous mode, the selection of models depends exclusively on what switches are active, which in turn depends on the modulation, which can be PWM, space vector, etc. However, if discontinuous modes exist, then the selection function must consider also the states. Consider the following modes on the boost converter:

- Mode 1: Equations (2.9) - (2.10)
- Mode 2: Equations (2.11) - (2.12)
- Mode 3: Equations (2.19) - (2.20)

When in mode 1, and the current falls to zero, it must jump to the model corresponding to the discontinuous conduction mode, mode 3. This behavior can be captured with a finite state machine as in figure 2.13.

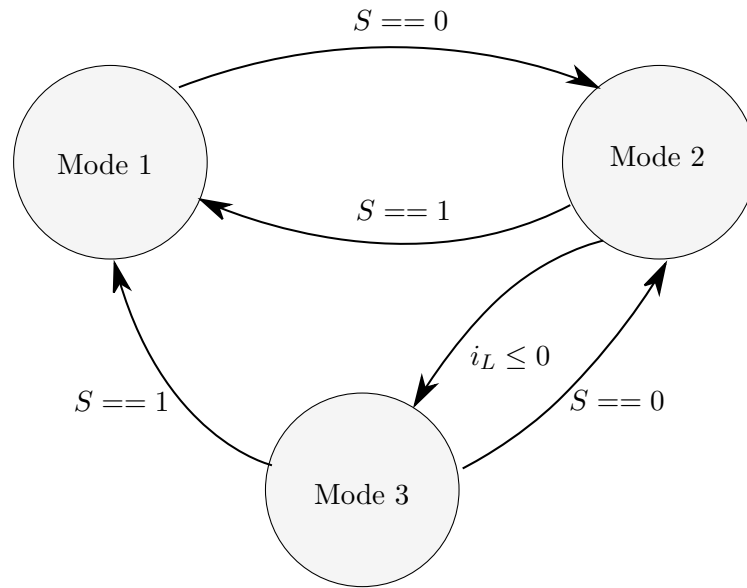


Figure 2.13: Automaton describing the behavior of the boost converter

Switching frequencies of a power converters are in the order of hundreds of kHz for small converters, and a few kHz or even hundreds of Hz for bigger converters.

This makes simulation of a few seconds a very computationally heavy task. For long simulation where the average behavior is more relevant an averaged model is used. The averaging of switched systems is covered in detail in [28], where the switching function in (2.21) plays a determinant role. Averaging of the converters in this work is covered in the next two sections for the DC-DC converter and the inverter.

2.4 Interleaved boost converter

The converter topology presented here is an interleaved bidirectional DC-DC converter. The interleaved term refers to the use of two or more branches of switching cells, properly shifted in phase to minimize current ripple. Furthermore, power may flow both ways in the converter, therefore is a bidirectional converter. Finally, DC-DC is in reference to the type voltage on both sides of the converter. This converter is the buffer between battery pack and inverter. This sections covers the modeling

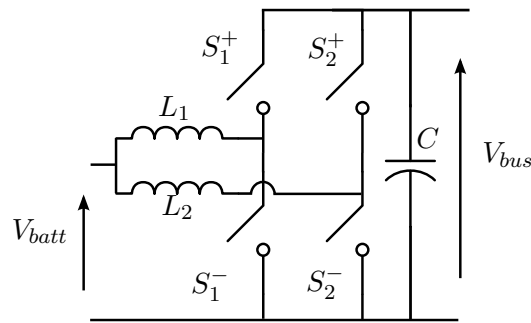


Figure 2.14: Bidirectional interleaved boost converter

of the converter. The modeling of the converter is done in two steps. A first step is a detailed analysis of the different modes of the converter. A converter may be viewed as a hybrid system, and in consequence it will go through a series of discrete states that in turn can be individually modeled as dynamical systems. To avoid confusion between the term state in the sense of state-space, and the discrete states of the hybrid system, the latter will be referred to as modes. Since the switching frequency of the converter is usually in the range of kHz, only the slow dynamics are of interest, i.e. the average dynamics. Consequently the next step is to obtain the average dynamics from the switched dynamics, what it is known as a Generalized Average Model (GAM) [27].

2.4.1 Switched model

To analyze the behavior of this converter, it is more convenient to start with a single branch. Once the concept has been grasped it may be expanded further. Some simplifying assumptions are made on top of the already stated in section 2.3:

- Inductances are designed so that they don't reach saturation
- Both switches in a single branch can't be closed at the same time
- Modulation is PWM.

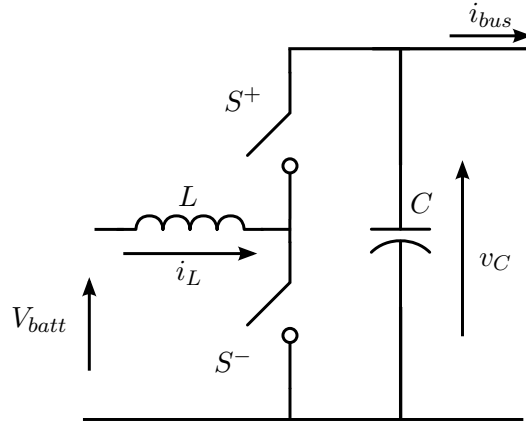


Figure 2.15: Bidirectional boost converter with a single branch

Following the procedure established in the previous section, and considering the previous assumptions, two modes can be identified. With equations:

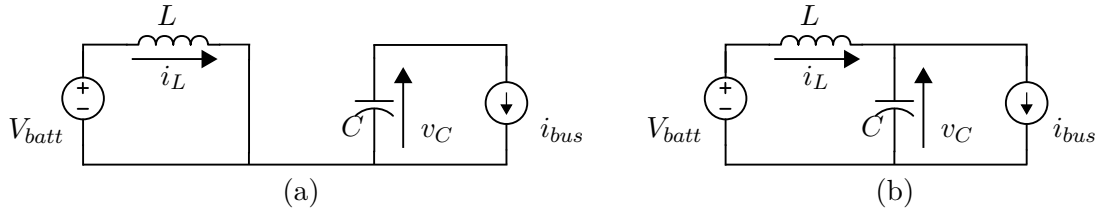


Figure 2.16: Modes: (a) Mode 1, (b) Mode 2

$$\text{Mode 1:} \quad (2.22)$$

$$\frac{di_L}{dt} = \frac{V_{batt}}{L} \quad (2.23)$$

$$\frac{dv_C}{dt} = -\frac{i_{bus}}{C} \quad (2.24)$$

$$\text{Mode 2:} \quad (2.25)$$

$$\frac{di_L}{dt} = \frac{V_{batt} - v_C}{L} \quad (2.26)$$

$$\frac{dv_C}{dt} = \frac{-i_{bus} + i_L}{C} \quad (2.27)$$

There exists yet another mode, a discontinuous conduction mode, possible when both switches are open at the same time. Since during normal operation that is

not possible, the mode has been ignored, which simplifies the analysis greatly. The outputs of the model are, as shown in 2.2 the battery current i_{batt} , and the bus voltage V_{bus} :

$$i_{batt} = i_L \quad (2.28)$$

$$V_{bus} = v_c \quad (2.29)$$

The converter as it is now, is indeed a simpler version of the boost converter shown in the previous section. As a matter of fact adding a second branch it is as simple as considering the new branch as an independent converter, sharing the state variable v_C and with $i_{batt} = i_{L_1} + i_{L_1}$.

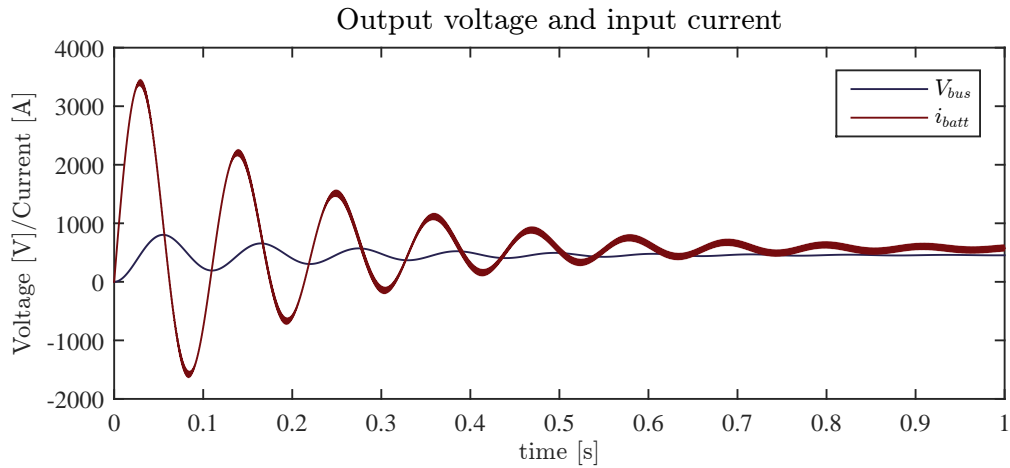


Figure 2.17: Output voltage and input current of the DCDC interleaved converter when started

Some simulation results are shown in figure 2.17. Figure 2.18 shows a detail of the current in the inductances of the converter. Notice how in the lower figure, the currents tessellate. This because the duty ratio is of 50%, i.e. the current in both branches show a perfectly shifted current. In the upper figure however, the duty cycle is of 20%, which results in the current ripple shown. This explain why is it important to work around on duty ratio of said value. Furthermore, the battery pack is designed so its voltage matches half the inverters nominal voltage.

2.4.2 Generalized average model

Because of the hybrid nature of power converters, it is difficult to design a controller based on the switched model. Certainly, some techniques exist to control said systems, as stabilization via a Common Lyapunov function [7]. However because of the

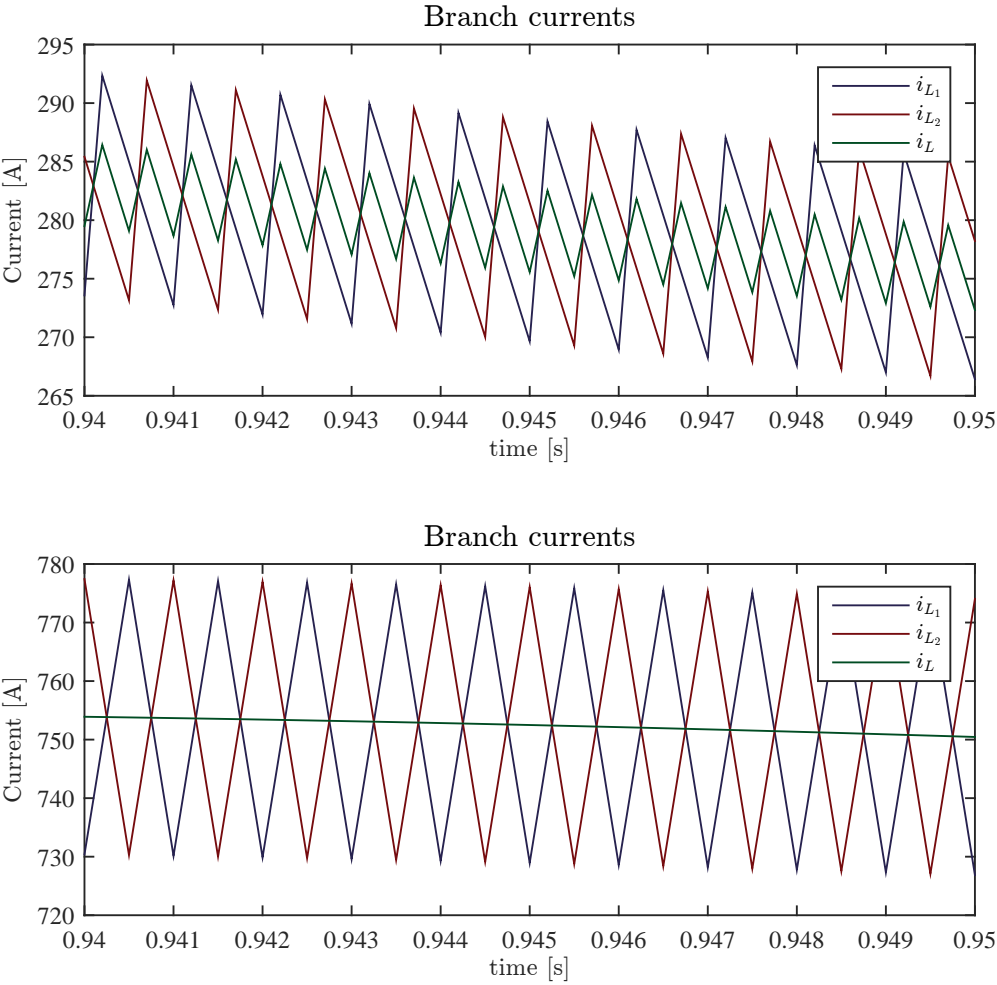


Figure 2.18: Tessellation of the inductor currents and current ripple

high switching frequency of these systems, it is not possible to develop a controller able to work between transitions. A different approach is to exploit this feature of converters to generate an average model from which a controller can be derived. This is possible due to the time-scale separation between the dynamics of the dynamical system and the time variations of the derivative of the states [28], that is, the switching from mode to mode (and therefore its associated continuous system) is faster than the global dynamics themselves.

Consider a switched system described by the following expression

$$\dot{x}(t) = \sum_{i=1}^m q_i(t) (A_i x(t) + B_i u(t)) \quad (2.30)$$

where:

- A_i is the A matrix of mode i
- B_i is the B matrix of mode i
- q_i is a selection function that may only take values 0 or 1
- x is the state vector
- u is the input vector

Under the assumption of constant cycle time, i.e. constant switching frequency, the averaged model of this system is computed as follows [28]

$$\dot{x}(t) = \int_{t-T}^t \sum_{i=1}^m q_i(s) (A_i x(s) + B_i u(s)) ds \quad (2.31)$$

Since

$$d_i(t) = \int_{t-T}^t q_i(s) ds \quad (2.32)$$

where $d_i(t)$ is the duty ratio of mode i

$$\dot{x}(t) = \sum_{i=1}^m d_i(t) (A_i x(t) + B_i u(t)) \quad (2.33)$$

which can be interpreted as a weighting of the modes based on how long time the system spends on each. The issue with this approach is its inability to capture higher dynamics of the system or AC behavior [28][27]. As a matter of fact, this "classical" averaged model is an special case of what is refer to in [27] as Generalized Averaged Model (GAM), or Dynamic Phasor Model in [28] and [30]. Under the scope of GAM approach, the classical averaged model would only consider the zero order harmonic, whereas the GAM considers an arbitrary number of harmonics. In the case of the interleaved converter, going for orders beyond the fundamental adds no intrinsic value

to the model itself. However since the procedure doesn't get overly convoluted when obtaining the GAM, it is still preferred, in the eventual case that the model wants to be extended.

Figure 2.19 shows the equivalent electrical diagrams of the converter in figure 2.14.

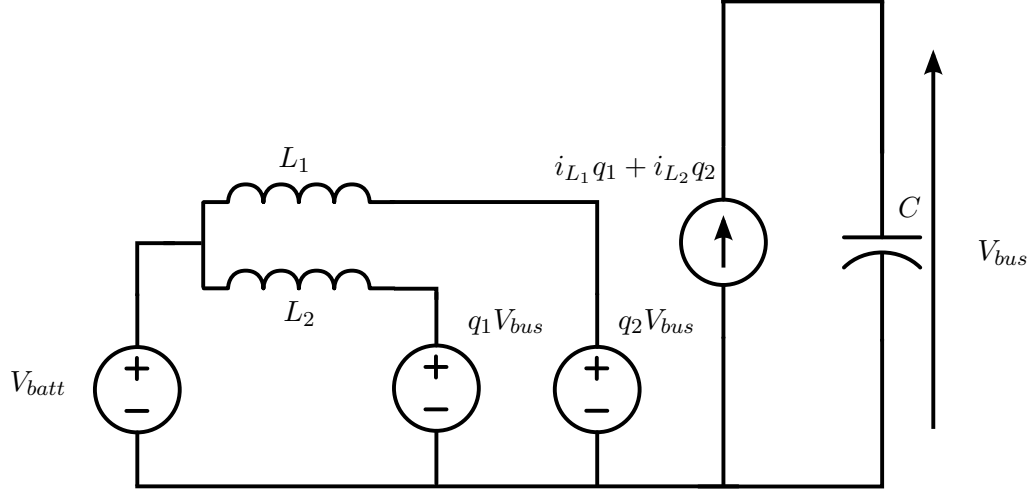


Figure 2.19: Bidirectional boost converter with a single branch

The converter has been separated in two by the switching branches. The circuit in the left side correspond to the battery side, while the right side is the bus side. The switching branches have been replaced by two voltage sources in the left-side and a current source in the right side. From the point of view of the inductances, when the switches are turned on and off, a voltage swinging from 0 to v_C appears on one of the ends. This can be seen by comparing equations (2.23) and (2.26). Similarly, on the capacitor side, it is seen as a current swinging from 0 to i_L . In the case of the interleaved converter, currents from both inductances go into the capacitor. Variables q_1 and q_2 are described by the switching functions. In this case switching functions of constant frequency and variable width. Variables q_1 and q_2 take values $\{0, 1\}$ depending on the state of S_1^+ :

$$q_i = \begin{cases} 1 & S_i^+ = 1, S_i^- = 0 \\ 0 & S_i^+ = 0, S_i^- = 1 \\ \text{not defined} & S_i^+ = 0, S_i^- = 0 \end{cases} \quad (2.34)$$

During normal operation it won't happen that both switches are open at the same time, thus no need to find a definition for q_i in that case. Writing the equations for

figure 2.19

$$\frac{di_{L1}}{dt} = \frac{1}{L} (V_{batt} - v_C q_1) \quad (2.35)$$

$$\frac{di_{L2}}{dt} = \frac{1}{L} (V_{batt} - v_C q_2) \quad (2.36)$$

$$\frac{dv_C}{dt} = \frac{1}{C} (i_{L1} q_1 + i_{L2} q_2 - i_{bus}) \quad (2.37)$$

The idea behind the GAM is to find the Fourier transform of the above equations

$$\langle x \rangle_k = \frac{1}{T} \int_{t-T}^t x(\tau) e^{-jk\omega\tau} d\tau \quad (2.38)$$

Notice how the transform in (2.38) is different from the usual transform in that this one is windowed over a period T , corresponding to the switching period. This is how the 'averaging' happens. Consider the 0 harmonic (i.e. $k = 0$), that's indeed the average value over a switching period. Additional harmonics capture higher order dynamics introduced by the switching. The transform (2.38) can be applied to equations (2.35) to (2.37) using the following expression, obtained from taking the time derivative of (2.38) [27]

$$\frac{d\langle x \rangle_k}{dt} = -jk\omega \langle x \rangle_k + \left\langle \frac{dx}{dt} \right\rangle_k \quad (2.39)$$

This expression shows an imaginary part for $k > 0$. As previously stated, for this converter, only the 0 harmonic is of interest (one could say, the DC component). However, if it were the case that an AC stage existed, harmonics of higher order would be relevant. In that case the imaginary part could be treated as an additional state variable. Now, applying (2.39) to (2.35)-(2.37)

$$\frac{d\langle i_{L1} \rangle_0}{dt} = \left\langle \frac{di_{L1}}{dt} \right\rangle_0 = \frac{1}{L} (\langle V_{batt} \rangle_0 - \langle v_C q_1 \rangle_0) \quad (2.40)$$

$$\frac{d\langle i_{L2} \rangle_0}{dt} = \left\langle \frac{di_{L2}}{dt} \right\rangle_0 = \frac{1}{L} (\langle V_{batt} \rangle_0 - \langle v_C q_2 \rangle_0) \quad (2.41)$$

$$\frac{d\langle v_C \rangle_0}{dt} = \left\langle \frac{dv_C}{dt} \right\rangle_0 = \frac{1}{C} (\langle i_{L1} q_1 \rangle_0 + \langle i_{L2} q_2 \rangle_0 - \langle i_{bus} \rangle_0) \quad (2.42)$$

As shown in [27]

$$\langle x \cdot y \rangle_k = \sum_i \langle x \rangle_{k-i} \langle y \rangle_i \quad (2.43)$$

then it follows for $k = 0$

$$\langle x \cdot y \rangle_0 = \dots + \langle x \rangle_1 \langle y \rangle_{-1} + \langle x \rangle_0 \langle y \rangle_0 + \langle x \rangle_{-1} \langle y \rangle_1 + \dots \quad (2.44)$$

$$\approx \langle x \rangle_0 \langle y \rangle_0 \quad (2.45)$$

It is also at this point, by neglecting the effect of the higher harmonics, where the "classical" averaged method may fail to properly capture the dynamics of the converter. Equations (2.40)-(2.42) can now be expanded

$$\frac{d\langle i_{L_1} \rangle_0}{dt} = \frac{1}{L} (\langle V_{batt} \rangle_0 - \langle v_C \rangle_0 \langle q_1 \rangle_0) \quad (2.46)$$

$$\frac{d\langle i_{L_2} \rangle_0}{dt} = \frac{1}{L} (\langle V_{batt} \rangle_0 - \langle v_C \rangle_0 \langle q_2 \rangle_0) \quad (2.47)$$

$$\frac{d\langle v_C \rangle_0}{dt} = \frac{1}{C} (\langle i_{L_1} \rangle_0 \langle q_1 \rangle_0 + \langle i_{L_2} \rangle_0 \langle q_2 \rangle_0 - \langle i_{bus} \rangle_0) \quad (2.48)$$

Now the Fourier transform of (2.38) can be applied to q_1 and q_2 separately. It should be noted that these are square signals with width t and period T such that:

$$d_i = \frac{t}{T} \quad (2.49)$$

Then their Fourier transform is:

$$\langle q_i \rangle_k = \begin{cases} d_i(t) & k = 0 \\ \frac{j}{k2\pi(e^{-jk2\pi d_i})} - 1 & k \neq 0 \end{cases} \quad (2.50)$$

where

$$d(t) = d_1(t) = d_2(t) \quad (2.51)$$

Where $d(t)$ is indeed the duty ratio, and the value of the DC component of switching function. Then the Generalized Average Model of the interleaved boost converter considering only the 0 harmonic is:

$$\frac{d\langle i_L \rangle_0}{dt} = \frac{2}{L} (\langle V_{batt} \rangle_0 - \langle v_C \rangle_0 d(t)) \quad (2.52)$$

$$\frac{d\langle v_C \rangle_0}{dt} = \frac{1}{C} (2\langle i_L \rangle_0 d(t) - \langle i_{bus} \rangle_0) \quad (2.53)$$

Writing it in matrix form and removing the notation for the Fourier transform of state variables:

$$\begin{bmatrix} \dot{i}_L \\ v_C \end{bmatrix} = \underbrace{\begin{bmatrix} 0 & -\frac{1}{L} \\ \frac{2}{C} & 0 \end{bmatrix}}_A \cdot \underbrace{\begin{bmatrix} i_L \\ v_C \end{bmatrix}}_x d + \underbrace{\begin{bmatrix} \frac{1}{L} & 0 \\ 0 & -\frac{1}{C} \end{bmatrix}}_D \cdot \underbrace{\begin{bmatrix} V_{batt} \\ i_{bus} \end{bmatrix}}_\delta \quad (2.54)$$

Notice that the state variables in this model are not the actual variables of the system, but their windowed harmonics.

2.4.3 Switched model vs. GAM

Simulation results are shown now comparing the GAM and the Switched mode. Figure 2.20 shows the switched model and GAM, where a step on the load has been performed at around the 1 second mark. It can be seen the GAM tracks almost perfectly the average dynamics.

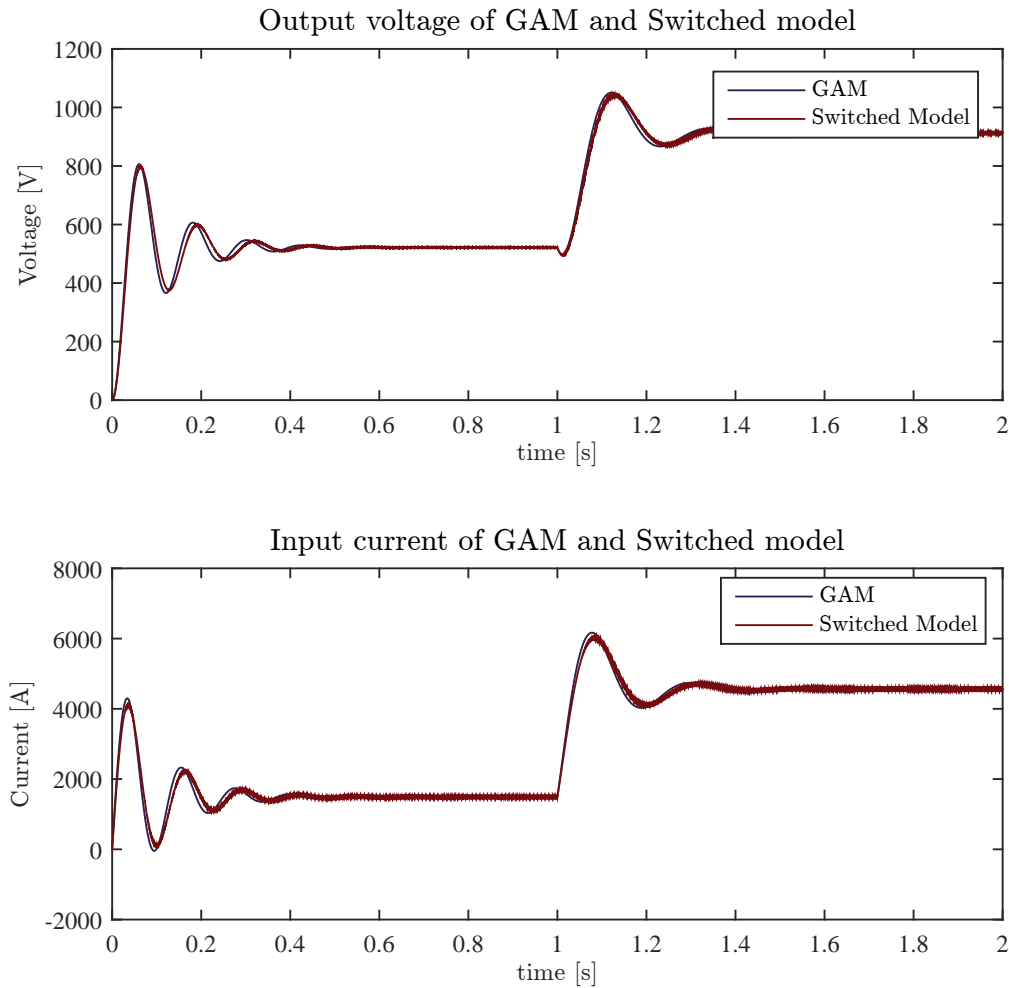


Figure 2.20: Comparison between the GAM and the switched model

An interesting detail that can be observed from the top figure, showing the output voltage of the converter, is that the ripple on the voltage also increases after the load step. Had the GAM also considered higher order harmonics, this change in ripple could have been accounted for. However the complexity that this would have added

to the model was deemed unnecessary. In converters with lower switching frequencies ($< 1\text{kHz}$), or lower inductances and capacitor values, the ripple can be rather high and have an important impact in the behavior of the converter. In those cases a higher order GAM would be justified.

2.5 SVM Inverter

The objective of this section is to describe the inverter. An inverter is a power electronics converter that transforms a DC voltage into an AC voltage of the desired amplitude and frequency. The figure shows the electrical diagram of said converter. Many variations of inverters exists. In this work a bi-level three-phase is covered. The two-level term refers to the number of voltage levels that can yield. This definition is rather arbitrary based on how this voltage levels are counted, therefore sometimes it can be found that this converter is referred to as a three-level converter. In the sequel it will be referred plainly as inverter.

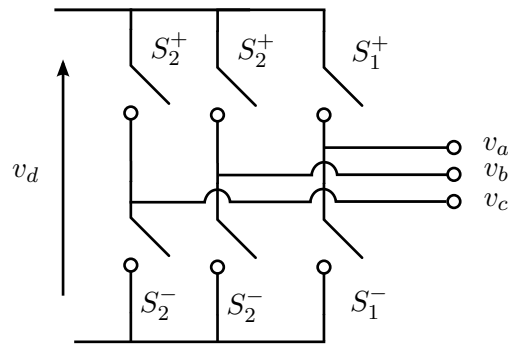


Figure 2.21: Inverter

Consider the converter in the figure, when switches S_1^+ and S_2^- , voltage between terminals V_a and V_b becomes:

$$v_{ab} = v_a - v_b = v_d \quad (2.55)$$

If, on the other hand S_1^- and S_2^+ are closed, then:

$$v_{ab} = -v_d \quad (2.56)$$

Thus, with the right combination of switches an alternating voltage can be obtained from a positive voltage. It only remains to find the appropriate switching sequence to obtain a voltage of the desired amplitude and frequency. This is determined by the modulation. An example would be PWM. A three phase sinusoidal can be compared against a triangular signal, that in turn would trigger the corresponding switch. However industry standard is what is known as Space Vector Modulation (SVM) that

| Switching combination | Space Vector | v_{ab} | v_{bc} | v_{ca} | v_α | v_β |
|-------------------------------|--------------|----------|----------|----------|-------------------|--------------------------|
| $\bar{S}_1\bar{S}_2\bar{S}_3$ | v_0 | 0 | 0 | 0 | 0 | 0 |
| $S_1\bar{S}_2\bar{S}_3$ | v_1 | v_d | 0 | $-v_d$ | v_d | 0 |
| $S_1S_2\bar{S}_3$ | v_2 | 0 | v_d | $-v_d$ | $\frac{1}{2}v_d$ | $\frac{\sqrt{3}}{2}v_d$ |
| $\bar{S}_1S_2\bar{S}_3$ | v_3 | $-v_d$ | v_d | 0 | $-\frac{1}{2}v_d$ | $\frac{\sqrt{3}}{2}v_d$ |
| $\bar{S}_1S_2S_3$ | v_4 | $-v_d$ | 0 | v_d | $-v_d$ | 0 |
| $\bar{S}_1\bar{S}_2S_3$ | v_5 | 0 | $-v_d$ | v_d | $-\frac{1}{2}v_d$ | $-\frac{\sqrt{3}}{2}v_d$ |
| $S_1\bar{S}_2S_3$ | v_6 | v_d | $-v_d$ | 0 | $\frac{1}{2}v_d$ | $-\frac{\sqrt{3}}{2}v_d$ |
| $S_1S_2S_3$ | v_7 | 0 | 0 | 0 | 0 | 0 |

Table 2.1: Output voltages for each switching combination and the $\alpha\beta$ equivalent. $S_n = 1$ and $S_n = 0$ are referred to as S_n and \bar{S}_n respectively.

will be covered in the sequel. The reason for SVM to be preferred over PWM has to do both with bus voltage utilization, as shown in [2], and lower harmonic content of the resulting signal.

Since both switches in a single branch cannot be closed at the same time, the state of a branch can be summarized as:

$$S_n = \begin{cases} 1 & S_n^+ = 1; S_n^- = 0 \\ 0 & S_n^+ = 0; S_n^- = 1 \end{cases} \quad (2.57)$$

Table 2.1 covers all possible switch combinations and its respective voltage output. The rationale behind SVM is each switch combination can be represented as voltage vectors in $\alpha\beta$ coordinates. This is shown in figure 2.22 and table 2.1. For the converter under study, there exist 6 active vectors, v_1 through v_6 , and two null vectors v_0 and v_7 . Voltage references to the inverter are given in $\alpha\beta$, and it is reconstructed as a linear combination of the three closest realizable vectors. For instance, a reference voltage $v_{\alpha\beta}^*$ that falls between vectors v_1 and v_2 will be produced

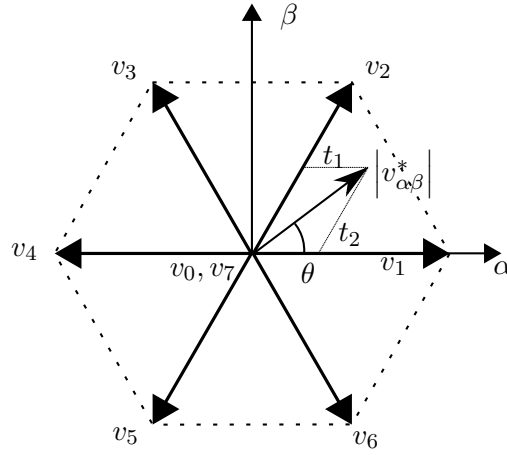


Figure 2.22: Space vector disposition in the $\alpha\beta$ axis. Notice vectors v_0 and v_7 are in the origin.

by switching between this vectors as follows:

$$v_{\alpha\beta} = v_1 t_1 + v_2 t_2 + v_0 t_0 \quad (2.58)$$

$$t_1 = \frac{|v_{\alpha\beta}^*|}{\frac{\sqrt{3}v_d}{2}} T_{sw} \sin\left(\frac{\pi}{3} - \theta\right) \quad (2.59)$$

$$t_2 = \frac{|v_{\alpha\beta}^*|}{\frac{\sqrt{3}v_d}{2}} T_{sw} \sin(\theta) \quad (2.60)$$

$$t_0 = T_{sw} - t_1 - t_2 \quad (2.61)$$

where:

| | | |
|-----------------------|--|-------|
| t_n | is the time spent in vector v_n | [s] |
| $ v_{\alpha\beta}^* $ | is the amplitude of the reference signal | [V] |
| θ | is the angle of the reference signal | [rad] |
| v_d | is the bus voltage | [V] |

The maximum achievable voltage amplitude $|v_{\alpha\beta}|_{max}$ corresponds to the voltage lying in the circle inscribed inside the hexagon in figure 2.22, that is:

$$|v_{\alpha\beta}|_{max} = \frac{\sqrt{3}}{2} v_d \quad (2.62)$$

Since the switches are ideal, the simulation model of the inverter reduces to a mapping from the bus voltage v_d to the output voltages v_{ab} , v_{bc} , v_{cd} defined by the modulation, as follows:

$$v_{ab} = v_d (S_1(t) - S_2(t)) \quad (2.63)$$

$$v_{bc} = v_d (S_2(t) - S_3(t)) \quad (2.64)$$

$$v_{ca} = v_d (S_3(t) - S_1(t)) \quad (2.65)$$

where the switching signals S_1 through S_2 are determined by the times in (2.59)-(2.59). Furthermore, the bus current i_d , can be computed from the load currents i_a , i_b and i_c and the switching at each instant, as follows:

$$i_d = i_a(t)S_1(t) + i_b(t)S_2(t) + i_c(t)S_3(t) \quad (2.66)$$

While the load currents $i_{abc}(t)$ are of course determined by the connected load:

$$\frac{di_{abc}}{dt} = f(t, i_{abc}, v_{abc}) \quad (2.67)$$

where

$$v_{abc} = \begin{bmatrix} v_{ab} \\ v_{bc} \\ v_{ca} \end{bmatrix} \quad (2.68)$$

The voltage produced is then a combination of steps, that on average resemble the reference voltage. The reference voltage $v_{\alpha\beta}^*$ is shown together with the actual output voltage in figure 2.23. The resulting current for an inductive load is shown as well. It

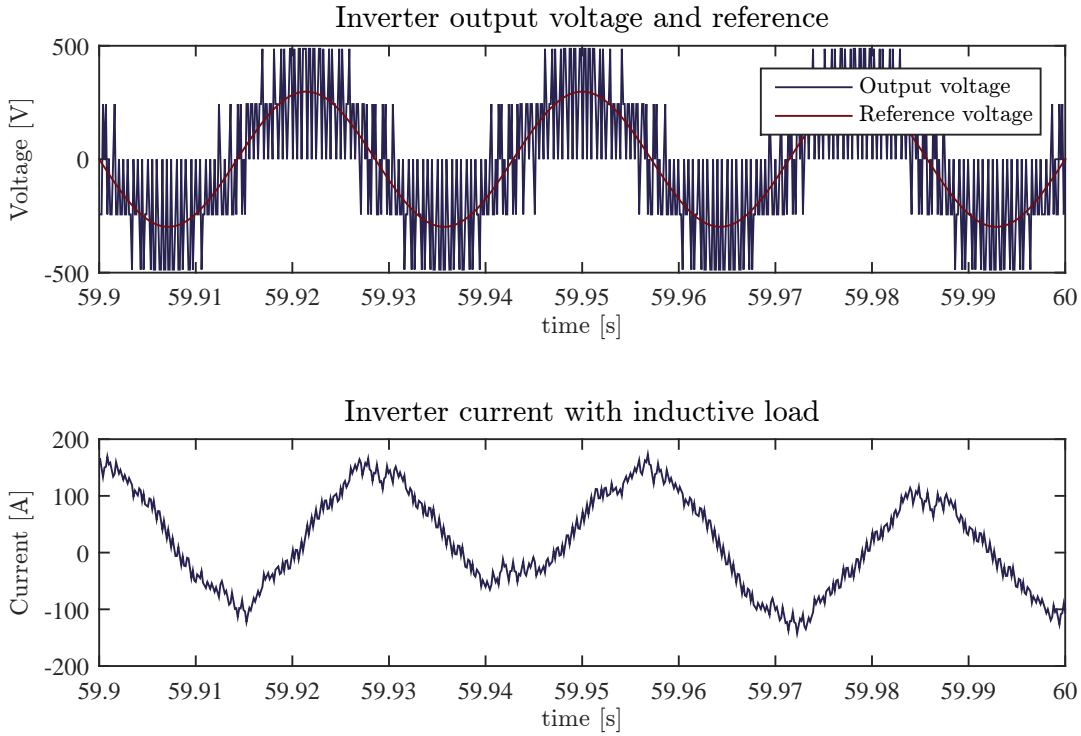


Figure 2.23: Output inverter voltage and current

should result obvious then that the inverter doesn't have dynamics of itself, and just

defines a mapping from v_d to v_{abc} and from i_{abc} to i_d as shown by equations (2.63) - (2.66). As a result, the averaged model of the inverter reduces to assuming that it can indeed reproduce any voltage reference ideally.

2.6 Induction Machine

An induction or asynchronous motor is an electrical machine that transforms electrical energy into mechanical energy. The machine was invented by Nikola Tesla and Galileo Ferraris independently in 1887 and 1885 respectively. An induction motor works by generating a rotating magnetic field by means of a set of coils in its stators. These coils are effectively placed 120° from each other (Figure 2.24), which coincides with phase shift in a three phase voltage. The magnetic field revolves at the speed of the frequency of the supplied electric voltage. The rotor of the induction machines consists in a series of coils connected to each other, oriented towards those of the stator. As a matter of fact, the most common design of the rotor is the one known as squirrel cage. It consists of two rings connected by spokes, and it resembles the aforementioned cage. Because of the rotating field in the stator, currents appear in the rotor, that in turn produces its own magnetic field (back mmf). The interaction between these magnetic fields generates a force that makes the rotor turn. Since the voltage on the rotor will only appear when it is subjected to a magnetic field of varying magnitude, if the rotor reaches synchronous speed, i.e. the same speed as the rotating field generated by the stator, no current appears in the rotor, and no back mmf exists and no torque generation. This means that the induction machine won't reach synchronous speed, thus the name, asynchronous motor. Furthermore, the difference between the rotor speed and the synchronous speed is called slip. Generally speaking, the higher the slip, the stronger the generated torque.

The model for the induction machine is well established, and ample information can be found in the literature [1][32][13]. However, the explanations given in [33] are clear and concise, and it has been reference followed for the sequel. Regardless, it must be said that it is the same model as the one presented in the other given references.

The model presented in this paper makes some assumptions, as follows:

- Iron losses are neglected
- Magnetic saturation is neglected

Both are difficult to quantify and are dependent on the temperature. Iron losses are usually small and difficult to model. While magnetic saturation introduces additional non-linearities in the equations due to the B-H curve, machines are designed to stay within the linear part of the curve during normal operation.

2.6.1 Three phase model equations

A set of variables are first defined for the physical magnitudes that play a role in the model:

$$u = \begin{bmatrix} u_a \\ u_b \\ u_c \end{bmatrix} \quad i = \begin{bmatrix} i_a \\ i_b \\ i_c \end{bmatrix} \quad \psi = \begin{bmatrix} \psi_a \\ \psi_b \\ \psi_c \end{bmatrix}$$

Being u , i and ψ the stator's voltage, current and linkage flux respectively. Current and flux are related as follows:

$$\psi = L(\theta) \cdot i \quad (2.69)$$

where:

θ the position of the rotor [rad]
 $L(\theta)$ is the inductance matrix [H]

The inductance matrix is a 3 dimension square matrix with varying parameters that describes the magnetic path between phases in the stator. The voltage equations in the stator are:

$$u = R \cdot i + \frac{d\psi}{dt} \quad (2.70)$$

where:

R is a diagonal matrix [Ω]

The first term accounts for the voltage drop due to the electric resistance of electric circuit. The second term is the voltage induced by the magnetic fields of the machine. The inductance matrix determines the contribution of each magnetic field to the voltage. The torque is given by:

$$T_{em} = \frac{1}{2} i^T \frac{dL(\theta)}{d\theta} i \quad (2.71)$$

where:

T_{em} is the electromagnetic torque [$\text{N} \cdot \text{m}$]

In the case of balanced operation, the following expression holds:

$$i_a + i_b + i_c = 0 \quad (2.72)$$

Meaning that one of the currents can be expressed using the other two. From here it can be deduced that a reduction of the model is possible without loss of generalization. This is indeed the case, and the resulting model is known as 2-phase model of the induction machine.

2.6.2 2-phase model

An induction machine has 3 coils distributed on its circumference. Each one produces a magnetic fields of varying magnitude. The resulting field is the rotating magnetic field that drives the rotor. Consider its three components:

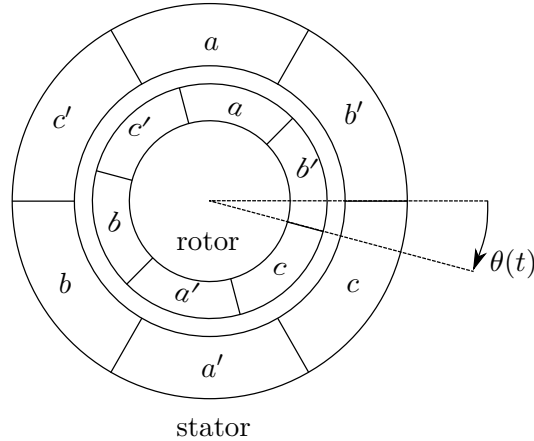


Figure 2.24: Relative position of the stator and rotor coils. Entry points of the coils are denoted a, b, c while the reciprocal are denoted a', b', c'

$$F_{abc} = \begin{bmatrix} F_a \\ F_b \\ F_c \end{bmatrix}$$

Where the magneto-motive force (mmf) F is:

$$F_s = N \cdot i \quad (2.73)$$

where:

N number of turns $[\]$

Because of (2.73) and (2.72), F_{abc} can be expressed using only two axis, as long as N is the same for each phase, which is true all motors. This is done by imposing two $\alpha\beta$ axes over the abc axes, as in figure 2.25 . The projection of abc over $\alpha\beta$ gives

$$\alpha_0 = a_0 - \frac{1}{2}b_0 - \frac{1}{2}c_0 \quad (2.74)$$

$$\beta_0 = -\frac{\sqrt{3}}{2}b_0 + \frac{\sqrt{3}}{2}c_0 \quad (2.75)$$

Since the resulting mmf is the same, a 3-phase machine can be represented by a 2-phase. Consider now the following equations for the 2-phase machine.

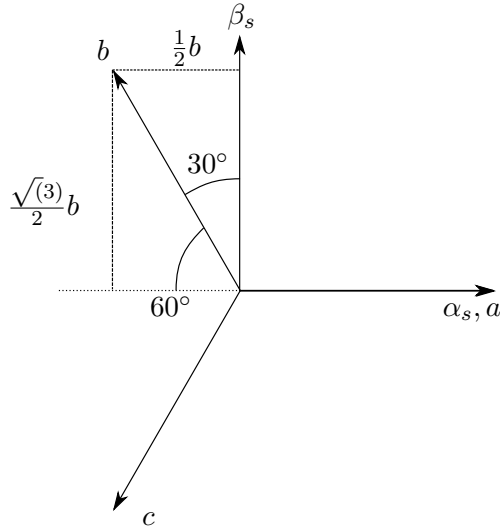


Figure 2.25: Projection of the abc axis over the $\alpha\beta$ axis

These are the stator equations:

$$u_{\alpha_s} = R_s i_{\alpha_s} + \frac{d\psi_{\alpha_s}}{dt} \quad (2.76)$$

$$u_{\beta_s} = R_s i_{\beta_s} + \frac{d\psi_{\beta_s}}{dt} \quad (2.77)$$

And the rotor equations:

$$0 = R_r i_{\alpha_r} + \frac{d\psi_{\alpha_r}}{dt} \quad (2.78)$$

$$0 = R_r i_{\beta_r} + \frac{d\psi_{\beta_r}}{dt} \quad (2.79)$$

The relation between currents and fluxes is

$$\begin{bmatrix} \psi_{\alpha_s} \\ \psi_{\beta_s} \\ \psi_{\alpha_r} \\ \psi_{\beta_r} \end{bmatrix} = \begin{bmatrix} L_s & 0 & L_m \cos(\theta) & -L_m \sin(\theta) \\ 0 & L_s & L_m \sin(\theta) & -L_m \cos(\theta) \\ L_m \cos(\theta) & L_m \sin(\theta) & L_r & 0 \\ -L_m \sin(\theta) & L_m \cos(\theta) & 0 & L_r \end{bmatrix} \cdot \begin{bmatrix} i_{\alpha_s} \\ i_{\beta_s} \\ i_{\alpha_r} \\ i_{\beta_r} \end{bmatrix} \quad (2.80)$$

Finally the torque is computed as follows:

$$T_{em} = \frac{3}{2} p (\psi_{\alpha_s} i_{\beta_s} - \psi_{\beta_s} i_{\alpha_s}) \quad (2.81)$$

This model can be directly implemented for simulation. However since voltage and current are 3-phase, they need to be transformed using relations (2.74) and (2.75). This transformation is known as Clarke transformation and it is a transformation

from \mathbb{R}^3 to \mathbb{R}^3 . The missing term in the $\alpha\beta$ coordinates is γ , which is zero if the 3 phases are balanced. From abc to $\alpha\beta\gamma$, the transformation is:

$$T = \frac{2}{3} \begin{bmatrix} 1 & -\frac{1}{2} & -\frac{1}{2} \\ 0 & \frac{\sqrt{3}}{2} & -\frac{\sqrt{3}}{2} \\ \frac{1}{2} & \frac{1}{2} & \frac{1}{2} \end{bmatrix} \quad (2.82)$$

The inverse:

$$T^{-1} = \begin{bmatrix} 1 & 0 & 1 \\ -\frac{1}{2} & \frac{\sqrt{3}}{2} & 1 \\ -\frac{1}{2} & -\frac{\sqrt{3}}{2} & 1 \end{bmatrix} \quad (2.83)$$

The constant in front of the transformation matrix in (2.82) changes its properties. For now it is enough to say that when it is $\frac{2}{3}$, the transformation is invariant in terms of impedance and inductance [33]. This is important, because it means that the parameters of the 3-phase machine can be used directly for its 2-phase representation. As a drawback, the transformation is not power invariant. However, this is not an issue, as the following is always true:

$$P_{\alpha\beta} = \frac{2}{3} P_{abc} \quad (2.84)$$

As a final note, yet another transformation is often performed. It consists on establishing another reference frame, called dq0, that rotates with the rotor, thus eliminating the trigonometric and time dependent variables from the equations, which makes the design of a controller easier and it will be covered in the next section. The model in $\alpha\beta$ is only used for simulation. Of which some results are shown in 2.26. Notice in the lower figure, that when the motor reaches synchronism, the fluxes stabilize. This is because the rotor is now rotating at the same speed than the stator's electrical field.

2.7 Field Oriented Model

The model in coordinates $\alpha\beta$ has been established in the previous worksheet. The main issue with this model is the presence of trigonometric functions through the inductance matrix, which make the analysis complicated. To address this issue a transformation can be introduced that translates the system into a rotating reference frame, such that these trigonometric functions disappear. Furthermore, this section covers how the system is transformed into this new reference frame and its implications. A control strategy, known as Field Oriented Control (FOC), or also Vector Control, is derived from this model. This is covered in section 3.2.6.

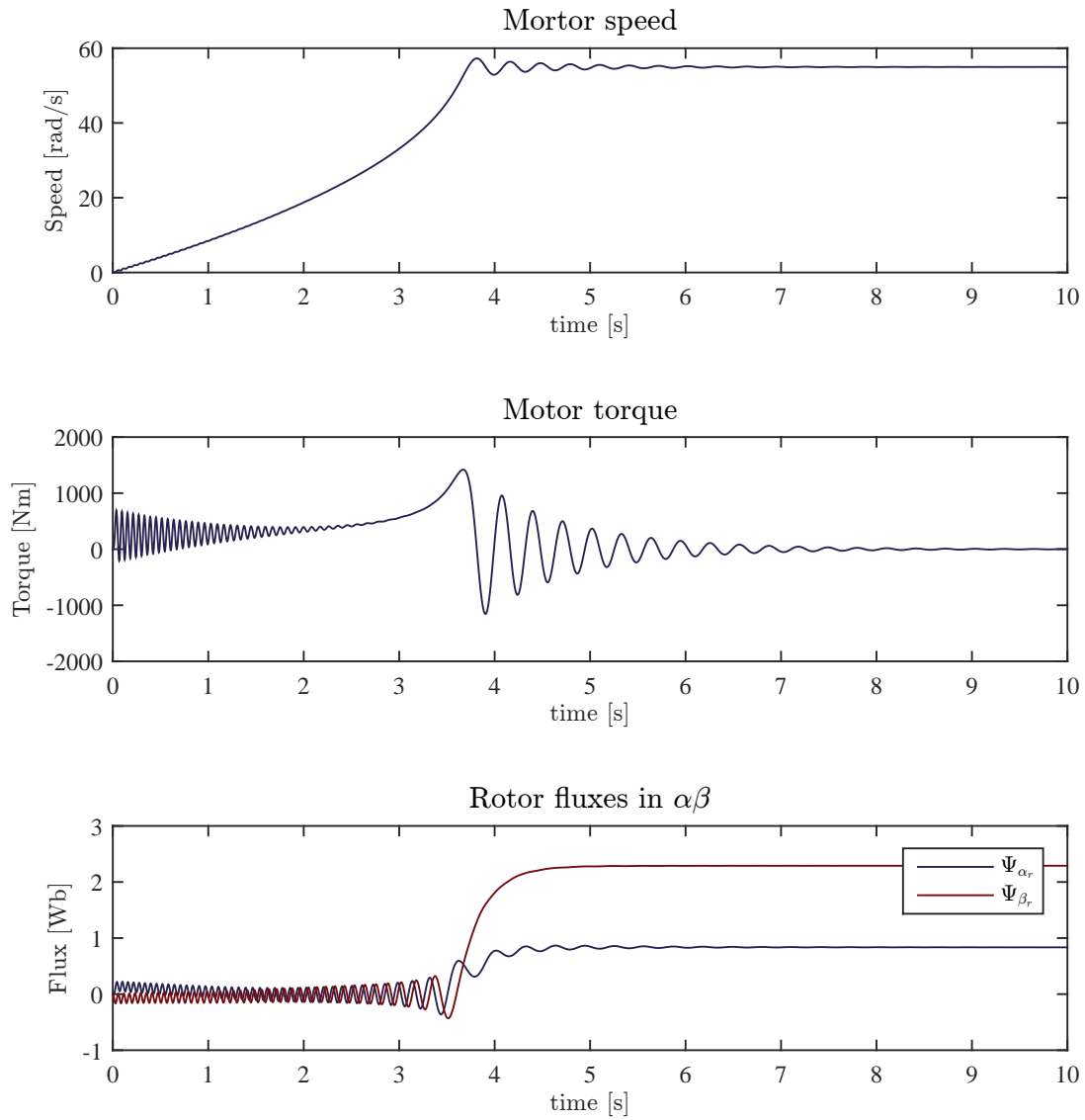


Figure 2.26: Simulation results of the induction motor. Voltage of constant magnitude and frequency is applied. The motor revs by itself up to synchronous (close) speed

2.7.1 Moving reference frame

Consider two sinusoidal currents i_α and i_β , in $\alpha\beta$ coordinates with frequency $\omega = \frac{d\theta}{dt}$. Since α and β are in quadrature, it can be written:

$$i_{\alpha\beta} = i_\alpha + ji_\beta \quad (2.85)$$

where j is the imaginary unit.

Now consider a frame dq rotating over $\alpha\beta$ at the same frequency ω as the currents. The currents i_α and i_β can then be projected onto dq , to obtain i_d and i_q

$$\begin{bmatrix} i_d \\ i_q \end{bmatrix} = \begin{bmatrix} \cos(\theta) & \sin(\theta) \\ -\sin(\theta) & \cos(\theta) \end{bmatrix} \cdot \begin{bmatrix} i_\alpha \\ i_\beta \end{bmatrix} \quad (2.86)$$

Or similarly

$$i_{dq} = i_d + ji_q = i_{\alpha\beta} e^{-j\theta} \quad (2.87)$$

In this new frame, as long as it rotates at the same frequency as the original currents, i_{dq} are not sinusoidal. Furthermore, would the frame dq be in phase with i_α , i_{dq} would then be the amplitudes of i_α and i_β . By applying this new frame to the $\alpha\beta$ model,

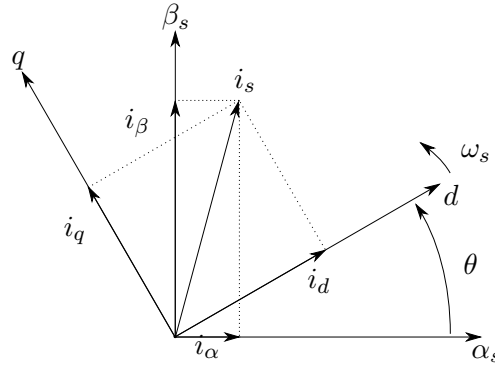


Figure 2.27: Projection of magnitudes in $\alpha\beta$ axis over the moving dq axis

the steady state sinusoidal behavior of the state variables can be removed. For the reader's sake, the model is repeated here.

The stator equations are

$$u_{\alpha_s} = R_s i_{\alpha_s} + \frac{d\psi_{\alpha_s}}{dt} \quad (2.88)$$

$$u_{\beta_s} = R_s i_{\beta_s} + \frac{d\psi_{\beta_s}}{dt} \quad (2.89)$$

And the rotor equations

$$0 = R_r i_{\alpha_r} + \frac{d\psi_{\alpha_r}}{dt} \quad (2.90)$$

$$0 = R_r i_{\beta_r} + \frac{d\psi_{\beta_r}}{dt} \quad (2.91)$$

The relation between currents and fluxes is

$$\begin{bmatrix} \psi_{\alpha_s} \\ \psi_{\beta_s} \\ \psi_{\alpha_r} \\ \psi_{\beta_r} \end{bmatrix} = \begin{bmatrix} L_s & 0 & L_m \cos(\theta) & -L_m \sin(\theta) \\ 0 & L_s & L_m \sin(\theta) & -L_m \cos(\theta) \\ L_m \cos(\theta) & L_m \sin(\theta) & L_r & 0 \\ -L_m \sin(\theta) & L_m \cos(\theta) & 0 & L_r \end{bmatrix} \cdot \begin{bmatrix} i_{\alpha_s} \\ i_{\beta_s} \\ i_{\alpha_r} \\ i_{\beta_r} \end{bmatrix} \quad (2.92)$$

It is convenient to have both rotor and stator equations in the same reference frame. It will be seen that when so, the variable inductance matrix of (2.92) will become constant.

To see that this is possible and still benefit from the advantages of a rotating frame, some investigation must be carried on. Let θ_s be the stator's current phase, then stator's frequency is

$$\frac{d\theta_s}{dt} = \omega_s \quad (2.93)$$

While the rotor's speed is

$$\omega_m = p \cdot \Omega \quad (2.94)$$

where:

$$\begin{array}{ll} p & \text{is the number of pairs of poles} \quad [\cdot] \\ \Omega & \text{is the mechanical speed of the shaft} \quad [\frac{\text{rad}}{\text{s}}] \end{array}$$

The induced currents in the rotor circuit then have frequency $\omega_{slip} = \omega_s - \omega_m$. This means that the current vector rotates around the rotor at frequency ω_{slip} , which in turn rotates at ω_m , therefore rotating at a total frequency of $\omega_{slip} + \omega_m = \omega_s$. Indeed, the rotor current vector (and therefore the flux vector) rotates at the same speed as the stator's, and by transforming rotor variables to a moving frame with speed ω_s , they will attain constant values at steady state.

Before transforming the rotor variables, it should be noted that in the $\alpha\beta$ model, the rotor variables were already expressed in a moving frame, that rotated with the rotor speed ω_m . As a matter of fact, in said model, if the motor would ever reached synchronous speed, then $\omega_{slip} = 0$ and $i_{\alpha\beta_r}$ would attain constant values. To transform the rotor variables to the new frame it can be done by multiplying the old variables by $e^{-j\theta_{slip}}$

$$i_{dq_r} = i_{\alpha\beta_r} \cdot e^{-j\theta_{slip}} \quad (2.95)$$

$$\psi_{dq_r} = \psi_{\alpha\beta_r} \cdot e^{-j\theta_{slip}} \quad (2.96)$$

While stator variables need to be multiplied by $e^{-j\theta_s}$

$$u_{dq_s} = u_{\alpha\beta_s} \cdot e^{-j\theta_s} \quad (2.97)$$

$$i_{dq_s} = i_{\alpha\beta_s} \cdot e^{-j\theta_s} \quad (2.98)$$

$$\psi_{dq_s} = \psi_{\alpha\beta_s} \cdot e^{-j\theta_s} \quad (2.99)$$

Because now rotor and stator variables are in the same frame, the inductances maintain their relative positions. Then the resulting inductance matrix is then

$$\begin{bmatrix} \psi_{d_s} \\ \psi_{q_s} \\ \psi_{d_r} \\ \psi_{q_r} \end{bmatrix} = \begin{bmatrix} L_s & 0 & L_m & 0 \\ 0 & L_s & 0 & L_m \\ L_m & 0 & L_r & 0 \\ 0 & L_m & 0 & L_r \end{bmatrix} \cdot \begin{bmatrix} i_{d_s} \\ i_{q_s} \\ i_{d_r} \\ i_{q_r} \end{bmatrix} \quad (2.100)$$

Applying Clarke's and then Parke's transformation to (2.92), or using equations (2.95) to (2.99), would result in the same.

Finally by substituting equations (2.95) - (2.99) into (2.88) - (2.91), the dq model of the induction machine is obtained

$$u_{d_s} = R_s i_{d_s} + \frac{d\psi_{d_s}}{dt} - \omega_s \psi_{q_s} \quad (2.101)$$

$$u_{q_s} = R_s i_{q_s} + \frac{d\psi_{q_s}}{dt} + \omega_s \psi_{d_s} \quad (2.102)$$

$$0 = R_r i_{d_r} + \frac{d\psi_{d_r}}{dt} - \omega_{slip} \psi_{q_r} \quad (2.103)$$

$$0 = R_r i_{q_r} + \frac{d\psi_{q_r}}{dt} + \omega_{slip} \psi_{d_r} \quad (2.104)$$

And the torque results in

$$T = \frac{3}{2} p (\psi_{q_r} i_{d_r} - \psi_{d_r} i_{q_r}) \quad (2.105)$$

2.7.2 Field Oriented Control

Field Oriented Control (FOC) of an induction machine, also referred to as Vector Control, is a control strategy that tries to force the induction machine to function as a doubly-fed DC machine, and therefore obtaining better torque response. This is achieved by using the rotor flux as the reference for the dq transformation, thus the name, field oriented. In figure 2.28, the cross section of a doubly-fed DC machine is shown. In this machine the flux ϕ_F is orthogonal to current I_A . It is the interaction between these two physical magnitudes that creates the force that causes the rotor to turn. Because of the construction of this machine, current I_A is always orthogonal to flux ϕ_F , and therefore the torque is constant. The idea behind FOC is that if the rotor's flux ψ_μ angle, or orientation, is known at all time, then the phase of the stator current vector i_s can be controlled to be orthogonal to the rotor's flux, achieving then constant torque. Additionally, by setting the reference to follow flux's orientation, i_{d_s} and i_{q_s} are effectively decoupled from the torque expression.

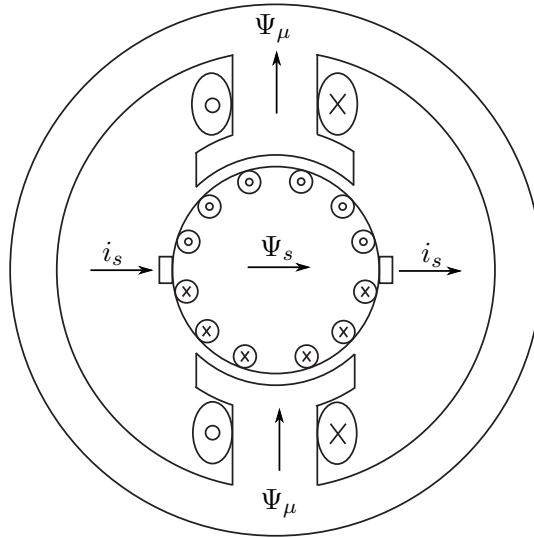


Figure 2.28: Cross section of a doubly-fed DC machine, and the would be equivalent variables in the induction machine

Starting with the rotor flux equations in (2.100), the d axis will be aligned with the rotor flux, then it must follow that

$$\psi_{q_r} = 0 = L_m i_{q_s} + L_r i_{q_r} \quad (2.106)$$

$$i_{q_r} = -\frac{L_m}{L_r} i_{q_s} \quad (2.107)$$

For ψ_{d_r} will capture the total rotor flux. This flux can be made proportional to some current i_μ . This can be interpreted as the magnetizing current of the rotor. Then it follows that

$$\psi_{d_r} = L_m i_{d_s} + L_r i_{d_r} \quad (2.108)$$

$$= L_m i_\mu \quad (2.109)$$

$$i_{d_r} = \frac{L_m}{L_r} (i_\mu - i_{d_s}) \quad (2.110)$$

Introducing this results in the rotor equations (2.103) and (2.104)

$$\omega_{slip} = \frac{R_r}{L_r} \frac{i_{q_s}}{i_\mu} \quad (2.111)$$

$$\frac{L_r}{R_r} \frac{di_\mu}{dt} + i_\mu = i_{d_s} \quad (2.112)$$

From (2.112) it can already be seen that the rotor flux now depends exclusively on i_d , meaning that by manipulating i_d , the magnitude of the rotor flux can be controlled.

Furthermore, the torque equation becomes

$$T = \frac{3}{2}p (\psi_{q_r} i_{d_r} - \psi_{d_r} i_{q_r}) \quad (2.113)$$

$$= \frac{3}{2}p \frac{L_m}{L_r} i_{q_s} \psi_{d_r} \quad (2.114)$$

In this new reference frame, as it can be deduced from observing equations (2.112) and (2.114), i_{q_s} regulates the torque, while i_{d_s} is the excitation current.

It is still necessary to transform the stator equations to this new frame. This is done by introducing (2.110) and (2.107) into the stator fluxes ψ_{d_s} and ψ_{q_s} , and these in turn into the stator equations (2.101) and (2.102)

$$u_{d_s} = R_s i_{d_s} + \sigma L_s \frac{di_{d_s}}{dt} + (1 - \sigma) L_s \frac{di_{\mu}}{dt} - \omega_s \sigma L_s i_{q_s} \quad (2.115)$$

$$u_{q_s} = R_s i_{q_s} + \sigma L_s \frac{di_{q_s}}{dt} + \omega_s (\sigma L_s i_{d_s} + (1 - \sigma) L_s i_{\mu}) \quad (2.116)$$

where σ is the total leakage coefficient [13][11] and equal to

$$\sigma = 1 - \frac{L_m^2}{L_s L_r} \quad (2.117)$$

It only remains to obtain the frequency ω_s . Since ω_{slip} is known from equation (2.111), and the motor speed ω_m can be measured

$$\omega_s = \omega_{slip} + \omega_m \quad (2.118)$$

$$= \frac{R_r}{L_r} \frac{i_{q_s}}{i_{\mu}} + \omega_m \quad (2.119)$$

Summarizing, the model in field oriented coordinates of the induction machine is

$$\text{Stator equations:} \quad (2.120)$$

$$u_{d_s} = R_s i_{d_s} + \sigma L_s \frac{di_{d_s}}{dt} + (1 - \sigma) L_s \frac{di_{\mu}}{dt} - \omega_s \sigma L_s i_{q_s} \quad (2.121)$$

$$u_{q_s} = R_s i_{q_s} + \sigma L_s \frac{di_{q_s}}{dt} + \omega_s (\sigma L_s i_{d_s} + (1 - \sigma) L_s i_{\mu}) \quad (2.122)$$

$$\text{Rotor equations:} \quad (2.123)$$

$$\frac{L_r}{R_r} \frac{di_{\mu}}{dt} + i_{\mu} = i_{d_s} \quad (2.124)$$

The new model decouples the rotor equations and allow for easier control of the motor through i_{d_s} and i_{q_s} . However stator equations are still coupled. Furthermore, magnitude and orientation of the rotor flux must be known for this controller be effective, which is not the case in many real world applications [11][1][13]. Thus a flux observer must be implemented. This, together with the controller design, is covered in section 3.2.6.

Chapter 3

Control objectives and design

3.1 Controller design: Industry Approach

The aim of this chapter is to cover the controllers designed for the system at hand. The approach taken is the same as in the industry, with a focus on pragmatism and no small amount of conservatism. However the first section, of this chapter, 3.2, starts with a topic slightly off the remain sections. It is the estimation of the batterie's state of charge by means of an Extended Kalman Filter. The differentiating aspect of it is that parameter estimation is also perform on-line by the filter, that treats two key parameters as states. In section 3.2.4 the design of a cascaded PI controller of the interleaved converter is covered. Section 3.2.6 covers the design of a Field Oriented Control (FOC) controller for the induction machine. Furthermore, an Extended Kalman Filter (EKF) has been designed to keep track of the non-measurable states. This part of the report concludes in section 3.2.10 with simulation results and a commentary on the performance of the controller.

As it is shown in figure 3.1, each subsystem is controlled independently. This strategy features a voltage regulator for the interleaved converter around some desired operating point, and a speed controller fro the induction motor. During acceleration, power is drawn from the bus, and the voltage drops. The voltage regulator will try to keep the voltage at the set-point value by drawing current from the battery. During braking, the opposite happens. Power is drawn from the motor into the bus. This causes the bus voltage to rise. Indeed, the voltage regulator, in order to keep the voltage at the set point, will pour the excess back into the battery. As it will be shown, this strategy is simple and effective, but it presents some drawbacks. During acceleration, the motor could benefit from higher bus voltage, however the opposite happens. Furthermore, no considerations on energy efficiency are done.

This control strategy resembles the industry usual approach, and examples may be found in many publications. This strategy features linear controllers, PID mostly,

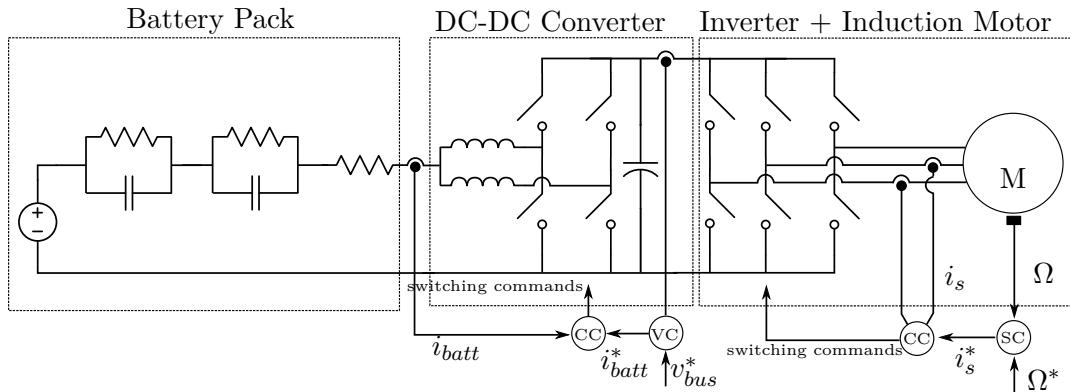


Figure 3.1: Diagram of the control structure described in this chapter. CC: Current controllers; VC: Voltage Controller; SC: Speed Controller

combined with heuristics to achieve the desired performance.

3.2 Battery state estimation

The objective of this section is to present an estimator for the battery so that the state of charge (SoC) can be known. Keeping track of the SoC is important as the voltage of the battery depends on it, and therefore has an impact in how much power can be delivered by it in any given instant. Furthermore, if the internal states of the battery can be observed, design of the controller for the converter attached will benefit.

The first approach consists on using a linear model to obtain the hidden states of the battery. The main objective of this estimation is indeed, to keep track of state of charge (SoC). A possible approach is just to integrate the current going in and out of the battery pack. This is known as Coulomb counting. Two issues with Coulomb counting are:

- Initial condition, i.e. initial SoC, may not be known, and therefore a permanent offset of the estimation will be carried over during the whole process.
- A priori, no feedback is available on the SoC, therefore the estimation will unavoidably deviate.

The first issue can ideally be addressed by keeping track of the Coulomb balance during the whole life of the battery. For obvious reasons this is highly unlikely to happen. Another approach would be to use those moments when the SoC of the battery is known to update the SoC, namely after a full charge or a full discharge.

However, depending on the application this may not happen at all.

The literature on SoC estimation is extense, yet no solution seems to have pushed through as a de facto standard. The most popular solution is the use of an Extended Kalman Filter (EKF) after an intensive characterizations of the cell as in [36]. As it is well known, batteries present many uncertainties and time-varying parameters, which in opinion of many authors, puts in question the robustness of said algorithm [3][16], who opt instead for H_∞ filters.

Since the exact modeling and characterization of a battery pack reaches out of the scope of this thesis, the design of the estimator will be carried under some simplifying assumptions:

- The battery pack is well known
- The history of the battery pack is also known
- Long term (month / years) aging effects over the battery pack are neglected.

The first assumption is fair, in which battery pack models are thoroughly characterized before its widespread use. For specimens of the same model obviously variations may exists, and that will be accounted for. The second and third assumption are related. Aging processes span for the total life of the battery. As the case study investigates the behavior of the system for periods of length from a few seconds to some tens of minutes, actual changes in the battery cannot be observed during operation. Furthermore, the second assumption implies the existence of a Battery Managing System (BMS) that keeps track of the history of the battery and slow changes in capacity, impedance,... etc.

For this reason and despite the well funded issues concerning robustness, the approach taken will make use of a EKF to keep track of the SoC. The main objective of the estimation is to obtain a good enough estimate of open circuit voltage (OCV), that as already stated in the previous worksheet is closely related with the SoC. To add some robustness to the estimation, on-line parameter estimation of the time constants in the battery model will be carried on.

3.2.1 Linear model and estimation

It is convenient to show first how the estimation work under close to ideal conditions to understand the relevance of a proper OCV-to-SoC mapping. For that, the

following linear model of the battery is used:

$$\begin{bmatrix} \dot{V}_{c_1} \\ \dot{V}_{c_2} \\ \text{SoC} \\ \dot{i} \end{bmatrix} = \underbrace{\begin{bmatrix} -\frac{1}{R_1 C_1} & 0 & 0 & \frac{1}{C_1} \\ 0 & -\frac{1}{R_2 C_2} & 0 & \frac{1}{C_2} \\ 0 & 0 & 0 & \frac{1}{C} \\ 0 & 0 & 0 & 0 \end{bmatrix}}_A \cdot \begin{bmatrix} V_{c_1} \\ V_{c_2} \\ \text{SoC} \\ i \end{bmatrix} \quad (3.1)$$

$$\begin{bmatrix} V \\ i \end{bmatrix} = \underbrace{\begin{bmatrix} 1 & 1 & K & 0 \\ 0 & 0 & 0 & 1 \end{bmatrix}}_C \cdot \begin{bmatrix} V_{c_1} \\ V_{c_2} \\ \text{SoC} \\ i \end{bmatrix} + \begin{bmatrix} V_{offset} \\ 0 \end{bmatrix} \quad (3.2)$$

where:

| | | |
|--------------|------------------------------------|-----------|
| A | is the state matrix | $[\cdot]$ |
| C | is the output matrix | $[\cdot]$ |
| K | is a constant that maps SoC to OCV | $[V]$ |
| V_{offset} | is the offset of the mapping | $[V]$ |

The model in (3.2) is linear. The current has been introduced as a state with zero dynamics in an effort to improve estimation as now the A matrix reflects how it is affected by it. Furthermore, the hysteresis effect over the OCV has been neglected and the nth degree polynomial substituted by a linear coefficient K . Figure ?? shows it's approximation

The following results put in highlight the importance of the SoC-to-OCV mapping and therefore the estimation of OCV. Non surprisingly, the Kalman Filter (not an EKF yet, since no nonlinearities have been accounted for in the model) performs well and it is able to estimate correctly the different states. More importantly, the results show that when the OCV can be observed the SoC can be corrected, even for completely disparate initial conditions. Obviously, as the OCV mapping has been approximated by a linear function the SoC extracted is not exact. A better approximation of this mapping may yield a better estimate of the SoC. The downside of relying so heavily on the OCV for SoC determination is that there is no such thing as a perfect characterization of its behavior, as it depends on temperature [31][19], history, and of course it changes slightly from battery to battery, even in the same model and chemistry. All in all, as long as the estimate is used with the due precaution it serves its purpose.

3.2.2 EKF and parameter estimation

As already mentioned, the robustness of the EKF is put in question because of its reliance on a model. When the issue are time varying parameters, the solution at hand is on-line estimation of said parameters. This works especially well when the variation of this parameters can be modeled and/or enough information is available

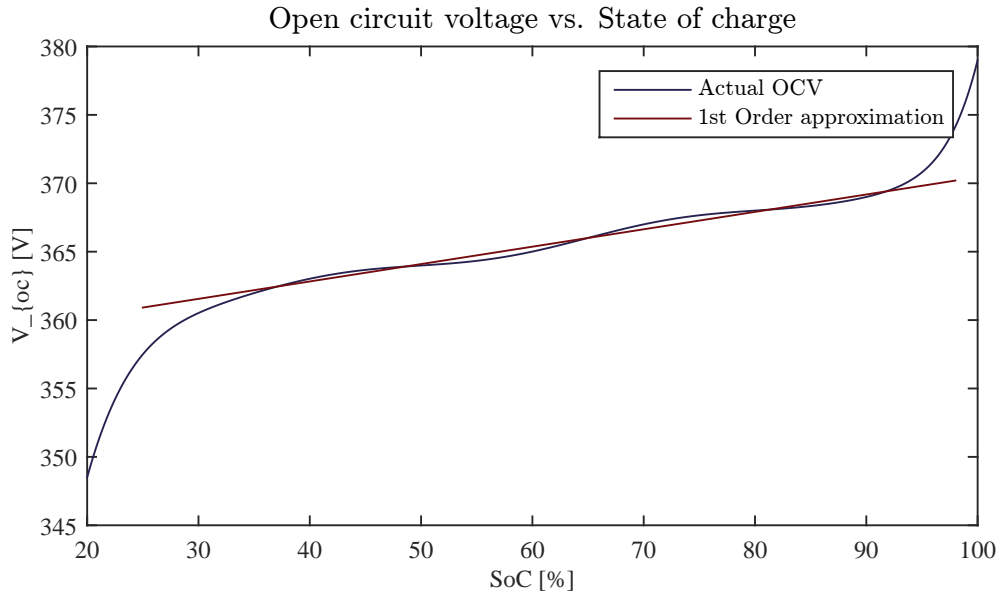


Figure 3.2: Insert Caption

to keep track of this changes, which doesn't seem to be the case for batteries. Efforts have been made to model changes due to temperature [31][14] and aging [29], which may help with estimation. Again the main issue with this approaches are the long and thorough characterization processes, not to mention that these are always done at cell level. When it comes to information available, the only direct measurements available are current and output voltage, and in the case that a thermal model would be available, temperature.

Not everything is lost however. The behavior of the battery may contribute to estimation to some degree. Under certain conditions some states can be observed better. Two cases can easily be shown with the following examples:

- During long rests (no current), the open circuit voltage can be observed directly through the output voltage
- Time constant separation in the battery allows for online identification when excited close to the proper frequency

The first example is self explanatory when (3.2) is considered. After a long rest, V_{c_1} and V_{c_2} will be close to zero, and therefore $V \approx K \cdot \text{SoC} + V_{offset}$. The second case depends on choosing time constants far enough apart and would only work under the assumption that enough excitation of the mode exists.

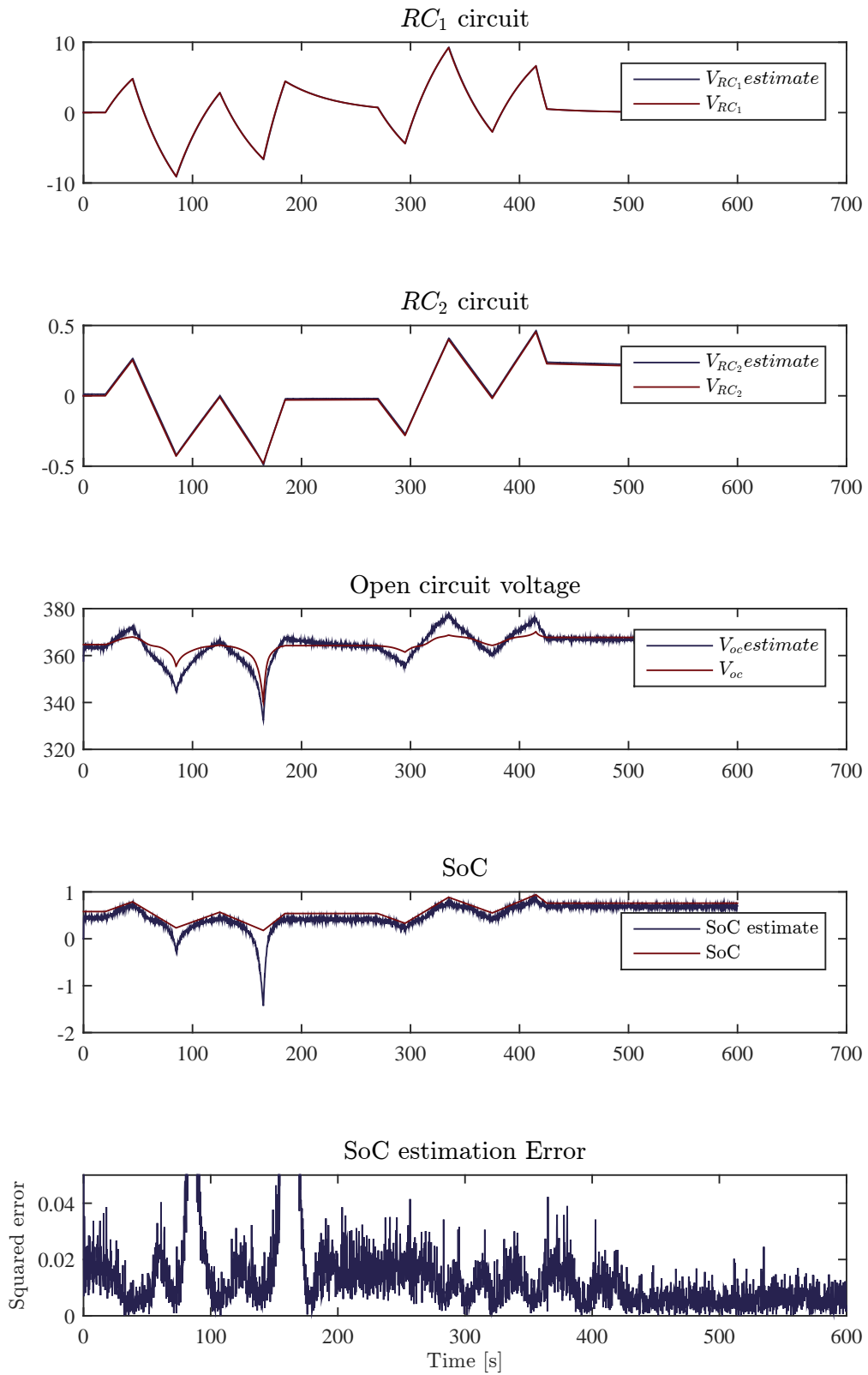


Figure 3.3: State estimation by the linear Kalman filter

All said, an EKF is implemented with an extended state vector that includes the time constants of the model.

$$A = \begin{bmatrix} -\hat{K}_{\tau_1} & -\hat{V}_{c_1} & 0 & 0 & 0 & \frac{1}{C_1} \\ 0 & 0 & 0 & 0 & 0 & 0 \\ 0 & 0 & -\hat{K}_{\tau_2} & -\hat{V}_{c_2} & 0 & \frac{1}{C_2} \\ 0 & 0 & 0 & 0 & 0 & 0 \\ 0 & 0 & 0 & 0 & 0 & \frac{1}{C} \\ 0 & 0 & 0 & 0 & 0 & 0 \end{bmatrix} \quad C = \begin{bmatrix} 1 & 0 & 1 & 0 & K & 0 \\ 0 & 0 & 0 & 0 & 0 & 1 \end{bmatrix} \quad (3.3)$$

$$x = \begin{bmatrix} V_{c_1} \\ K_{\tau_1} \\ V_{c_2} \\ K_{\tau_2} \\ \text{SoC} \\ i \end{bmatrix} \quad (3.4)$$

where:

$$\begin{aligned} K_{\tau_1} & \text{ is } \frac{1}{\tau_1} \quad [\text{s}^{-1}] \\ K_{\tau_2} & \text{ is } \frac{1}{\tau_2} \quad [\text{s}^{-1}] \end{aligned}$$

The equations are the same as (3.2). However with extension of the state vector, the matrices A and C must be extended in consequence.

3.2.3 Simulation results of the estimator

Simulation results are shown comparing the performance of the EKF with on-line parameter estimation to the Kalman Filter. Both estimators start with same initial conditions. The model parameters for both filters are not the actual parameters of the estimated system. The objective is to compare and determine if the on-line parameter estimation does indeed improve the estimation of the SoC. Figure 3.4 show the behavior of the estimator with on-line parameter estimation. It can be seen that the estimate of V_{RC_1} is accurate, while V_{RC_2} it is quite off all the time. This may easily be due to the lack of excitation on that frequency. The estimation of the open circuit voltage is as well rather off. Paradoxically, the estimate of SoC is rather accurate, except for the cases when the SoC wanders off the approximated OCV region, as around 180 seconds mark. Figure 3.5 shows how the estimate of the parameters go towards a different value than the actual. The explanation for this is that the filter is using them as a free variable to compensate for other model deviations, like the unaccounted histeresys effect or the approximation of the OCV. In the case for the Kalman filter with no parameter estimation, figure 3.3, the estimation of the different states is good even though the parameters are off. OCV presents less deviations than

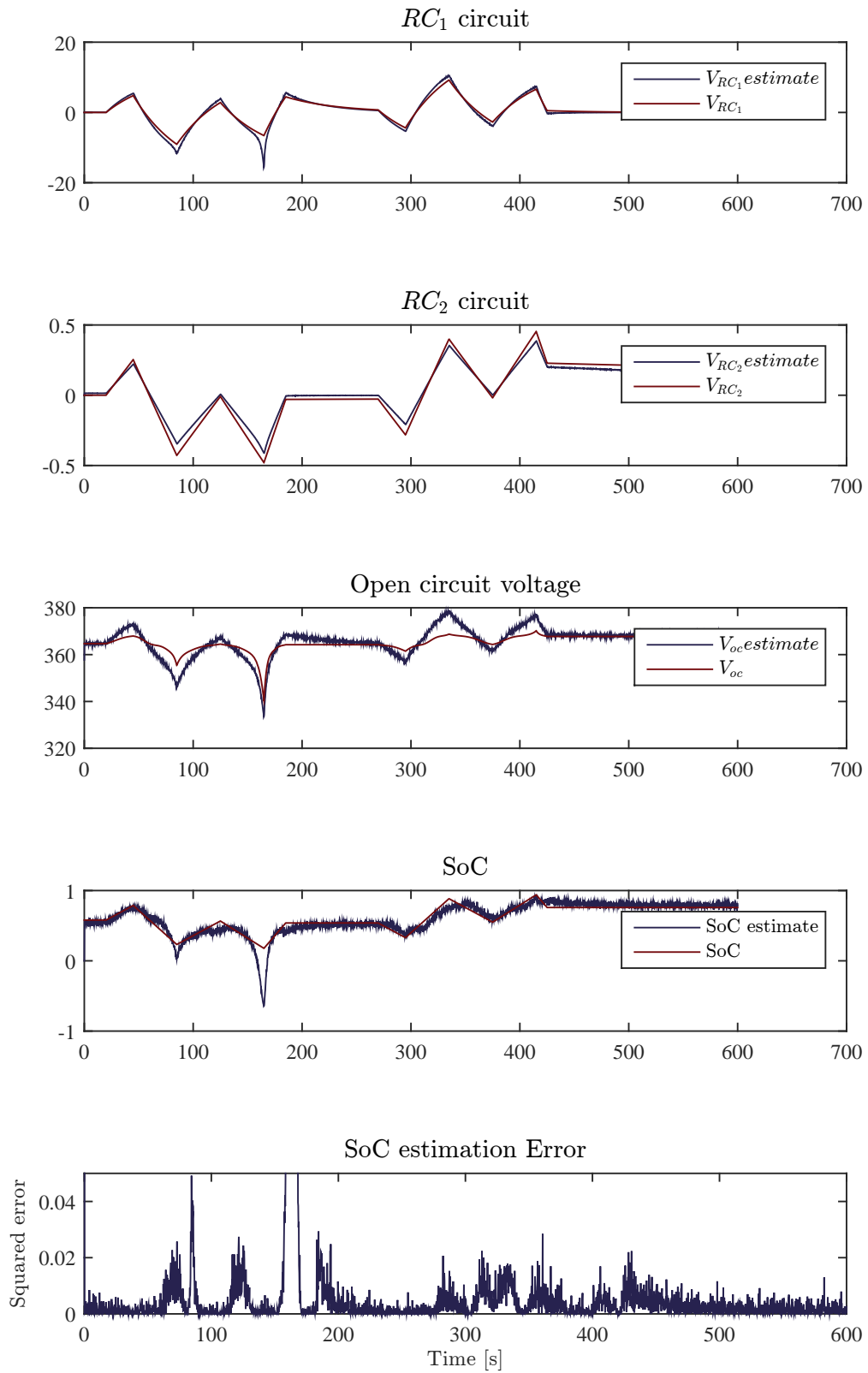


Figure 3.4: State estimation by EKF with online parameter estimation

in the parameter estimation case. However, the estimation of the SoC is quite off, compared to that of the parameter estimation case.

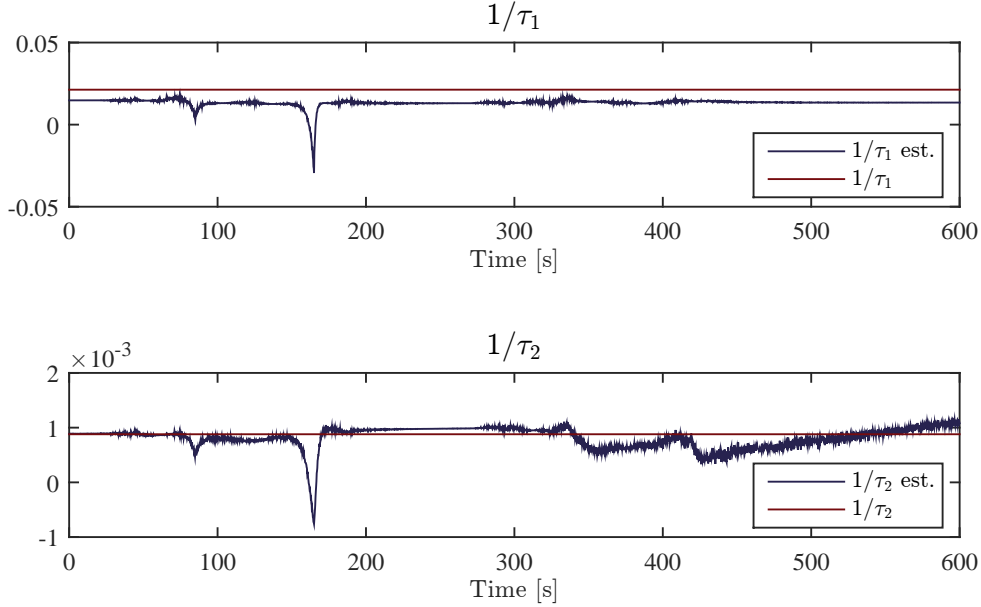


Figure 3.5: Actual value of the parameters and their respective estimates

3.2.4 Interleaved DC-DC converter

Recall the model of the averaged DC-DC converter (2.4.2), in section 2.4.2. It is repeated here:

$$\begin{bmatrix} \dot{i}_L \\ \dot{v}_C \end{bmatrix} = \begin{bmatrix} 0 & -\frac{1}{L} \\ \frac{2}{C} & 0 \end{bmatrix} \cdot \begin{bmatrix} i_L \\ v_C \end{bmatrix} \cdot d + \begin{bmatrix} \frac{1}{L} & 0 \\ 0 & -\frac{1}{C} \end{bmatrix} \cdot \begin{bmatrix} V_{batt} \\ i_{bus} \end{bmatrix} \quad (3.5)$$

where d is indeed the manipulated variable. Consider first the steady state characteristics of (3.5). By setting the derivative of the first equation to zero, the input output voltage ratio can be obtained:

$$\frac{v_C}{V_{batt}} = \frac{1}{d} \quad (3.6)$$

Remember that $d \in [0, 1]$. By inspecting the above equation, it can be deduced that a higher value of d , results in a lower input-output ratio. The complement \bar{d} of d is therefore introduced:

$$d = 1 - \bar{d} \quad (3.7)$$

As a result (3.5) yields:

$$\begin{bmatrix} \dot{i}_L \\ v_C \end{bmatrix} = \begin{bmatrix} 0 & -\frac{1}{L} \\ \frac{2}{C} & 0 \end{bmatrix} \cdot \begin{bmatrix} i_L \\ v_C \end{bmatrix} \cdot (1 - \bar{d}) + \begin{bmatrix} \frac{1}{L} & 0 \\ 0 & -\frac{1}{C} \end{bmatrix} \cdot \begin{bmatrix} V_{batt} \\ i_{bus} \end{bmatrix} \quad (3.8)$$

Under the assumption that the time constant associated to the current dynamics is smaller than that of the voltage, a cascade controller is presented, with an inner for the current, and an outer loop for the voltage. This is shown in the following figure. This is a common approach, derived from implementations where current control is

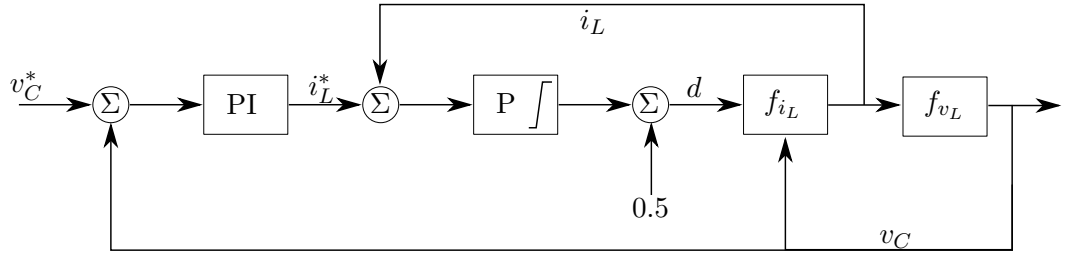


Figure 3.6: Cascaded controller, with a inner current loop and an outer voltage loop

implemented in hardware with high gains or even hysteresis control. A discrete implementation is of course possible as well. Additionally, this implementation permits the introduction of input current limitation, which is coherent with the needs of the battery. The present scheme uses a proportional controller for the current loop, and pure integral action in the voltage loop.

Following this logic a current feedback loop is designed. Starting with the first equation in (3.8):

$$\frac{di_L}{dt} = \frac{1}{L} (V_{batt} - v_C \cdot (1 - \bar{d})) \quad (3.9)$$

Consider the following control law:

$$\bar{d} = 0.5 - K\tilde{i}_L \quad (3.10)$$

with

$$\tilde{i}_L = i_L^* - i_L \quad (3.11)$$

where i_L^* is the set point. Furthermore, assume that the outer voltage loop does indeed work, and it is significantly slower than the current loop. Then i_L^* and v_C can be assumed constant. The same reasoning is applied to the battery behavior, resulting in that V_{batt} is assumed constant as well. When i_L is close to the reference

$\tilde{i}_L \approx 0$ and $\bar{d} \approx 0.5$. From the steady state analysis of (3.9) the ratio between V_{batt} and v_C is:

$$\frac{v_C}{V_{batt}} = \frac{1}{1 - \bar{d}} \quad (3.12)$$

which for $\bar{d} = 0.5$ results in $v_C = 2V_{batt}$. Furthermore, under the assumption that the outer loop is slow relative to the inner loop then $\frac{di_L^*}{dt} \approx 0$. All before considered, (3.9) becomes

$$\frac{d\tilde{i}_L}{dt} = \frac{v_C}{L} K \tilde{i}_L \quad (3.13)$$

$$\tilde{i}_L = e^{\frac{v_C}{L} K t} \quad (3.14)$$

$K < 0$ can be chosen to achieve the desired convergence rate. Of course in the presence of a non considered disturbance a steady state error will appear. Since the objective is control of the bus voltage, this is of no consequence. Furthermore, it is expected that the integral action in the voltage loop will compensate for it.

Assuming now that the current loop does indeed work, and that shows faster dynamics than the voltage loop, the bus capacitor voltage balance equation can be rewritten as:

$$\frac{dv_C}{dt} = \frac{1}{C} (i_L^* - i_{bus}) \quad (3.15)$$

In the same way introducing a proportional action stabilizes the system. Furthermore an integral action is introduced to compensate for the disturbance i_{bus} . Then:

$$i_L^* = K_P (v_C^* - v_C) + K_I \int_0^t v_C^* - v_C dt \quad (3.16)$$

Combining it with (3.15), the following system of equations is obtained:

$$\frac{dv_C}{dt} = \frac{1}{C} \left(K_P (v_C^* - v_C) + \tilde{i}_I - i_{bus} \right) \quad (3.17)$$

$$\frac{d\tilde{i}_I}{dt} = K_I (v_C^* - v_C) \quad (3.18)$$

By selecting K_P and K_I appropriately the convergence rate of the system towards the reference can be freely selected, as long as remains slower than the inner loop.

3.2.5 Simulation results

Some simulation results are now shown. Figure (3.7) shows the converter going from a voltage control mode, to a current control mode. An step on the voltage reference has been performed at on 4. The result is that for a constant load, the current will

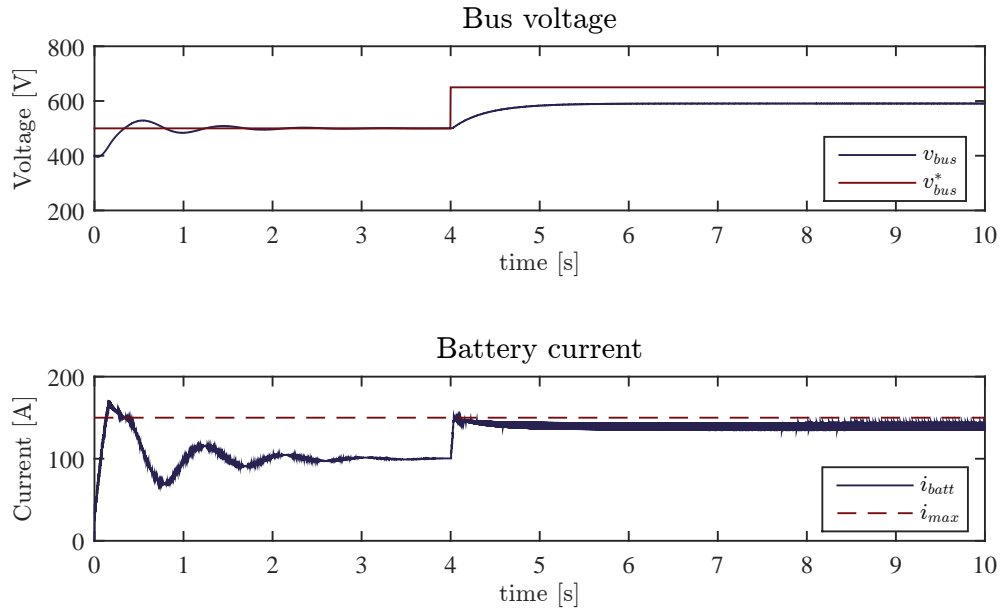


Figure 3.7: The inner loop takes the control once the voltage controller saturates

increase with the voltage. It happens however that the increase in current in the outgoing side, needs to be match with a current higher than the limit of 500A. The results is that the voltage loop saturates, and the current loop takes over. In figure 3.8 an step on the load has been carried on second 10. The current increases, this time below the saturation limit. Notice the effect on the voltage.

3.2.6 Induction Machine

In section 2.7 the idea behind Field Oriented Control was explained, and a model in field oriented coordinates was obtained. More specifically, the model was described in rotor flux coordinates. This point reached, many approaches to control the system exist in the literature. The most common approaches are known as direct and indirect FOC. The exact definition of each vary from source to source. In general, direct FOC refers to the case when all measurements are available, while indirect refers to the case when only speed and stator currents can be measured [13][1][23]. Many other approaches exists in the literature, these include the use of linear parameter variant controllers [10], passivity based controllers [23], and sliding mode controllers [21]. In the author's view, there are two reasons that motivate the existence of such variety of controllers for induction motors. First, the induction motor has been for many years, and still is, the workhorse in any industry that uses electrical motors, which encourages the search for ever improving performance. And second, even though the

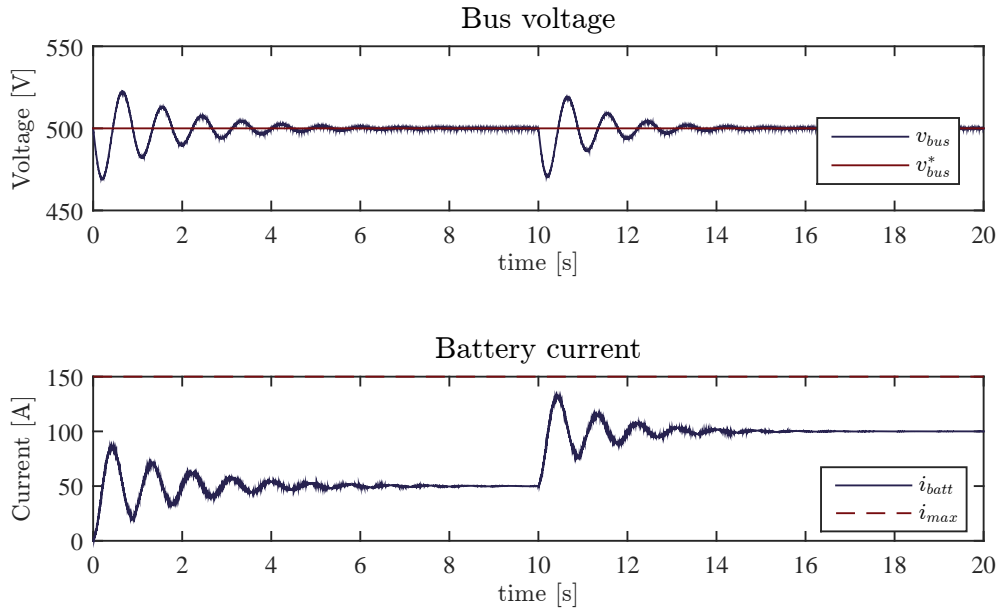


Figure 3.8: A step load is performed in the converter. The overshoot on the current propagates to the voltage

existing controllers are a usable solution, and a de facto standard exists, no controller yet exists that can address all the issues that the system presents. The objective of this section is therefore is to obtain a controller for the motor that present good enough performance in the application range, without wondering too deep in the existing state of the art.

One of the assumptions made during the development of the model for the induction machine, and therefore this controller, is time-invariance. This is not the case in a real motor, and it is in fact the motivation for many of the references cited above. Even when this feature is neglected, the system remains non-linear and complex enough to motivate the investigation of different approaches. As consequence two controllers are presented in this section. The first is a classical indirect FOC, as described in [1] and [13], but using a linear state feedback control law, instead of the more classical PID approach. For reference in the following sections, the model for

the motor as it was shown in section 2.7 is rewritten here in a more compact form:

$$\frac{di_d}{dt} = -\frac{R_s}{L_s\sigma}i_d - \frac{1-\sigma}{\sigma} \left(\frac{i_d - i_\mu}{\tau_r} \right) + \left(\frac{1}{\tau_r} \frac{i_q}{i_\mu} + \omega_m \right) i_q + \frac{1}{L_s\sigma}u_d \quad (3.19)$$

$$\frac{di_q}{dt} = -\frac{R_s}{L_s\sigma}i_q - \left(\frac{1}{\tau_r} \frac{i_q}{i_\mu} + \omega_m \right) i_d - \left(\frac{1}{\tau_r} \frac{i_q}{i_\mu} + \omega_m \right) \frac{1-\sigma}{\sigma}i_\mu + \frac{1}{L_s\sigma}u_q \quad (3.20)$$

$$\frac{di_\mu}{dt} = \frac{i_d - i_\mu}{\tau_r} \quad (3.21)$$

$$\frac{d\omega_m}{dt} = \frac{3}{2}p^2 \frac{L_m^2}{JL_r} i_q i_\mu - \frac{C}{J}\omega_m - \frac{p\tau_L}{J} \quad (3.22)$$

where:

τ_r is the time constant $\frac{L_r}{R_r}$ of the rotor's electrical circuit [s]

3.2.7 Indirect Field Oriented Control

Indirect FOC assumes that fine control of the stator currents i_d and i_q can be achieved. When this is true, the rotor magnetizing current i_μ can be independently controlled through i_d in equation (3.21). If i_μ is kept constant, then the torque, first term in the right-hand side of (3.22), is proportional to i_q . Indeed looking at equations (3.19) and (3.20), to find a controller for i_d , i_q may prove challenging. Furthermore, current i_μ is not available as a measurement, and needs to be estimated.

A solution to the control of currents i_d and i_q is hardware implemented high-gain current loops [13]. This is suitable for high frequency inverters [1], with switching frequencies in the order of the tens of kHz, and current source inverters (CSI). Unfortunately the inverter considered here runs closer to 1 kHz for efficiency reasons. Therefore, the current dynamics must be accounted for. In the figure above, the diagram for the classical implementation of indirect FOC is shown. The idea is to cancel the non-linear terms in equations (3.19) and (3.20) by using the following expressions:

$$u_d = L_s\sigma \left(v_d - \left(\frac{1}{\tau_r} \frac{i_q}{i_\mu} + \omega_m \right) i_q \right) \quad (3.23)$$

$$u_q = L_s\sigma \left(v_q + \left(\frac{1}{\tau_r} \frac{i_q}{i_\mu} + \omega_m \right) i_d + \omega_m \frac{1-\sigma}{\sigma} i_\mu \right) \quad (3.24)$$

where:

v_d is the auxiliary input signal for the d axis [V]

v_q is the auxiliary input signal for the q axis [V]

Indeed this decoupling, as it is referred to in the literature, assumes that a perfect cancellation can be achieved. However i_μ must be estimated, and convergence

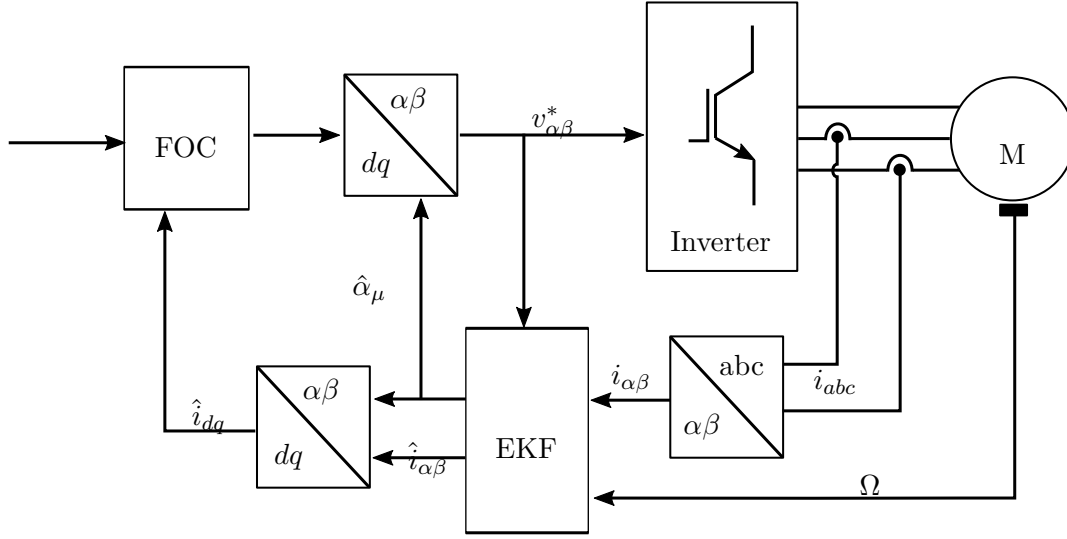


Figure 3.9: Control structure of FOC controller

of the estimate towards the actual value is asymptotic at best, and so will be the decoupling, as pointed out in [23]. Furthermore, during implementation, the exact value of τ_r can not be known, as R_r is highly dependent on the temperature. The consequence is loss of performance, but not of stability, as it was shown in [35] that the method is globally stable, allowing for a 200% error in the estimate of R_r .

After the decoupling, the resulting system is linear:

$$\frac{di_d}{dt} = -\frac{R_s}{L_s\sigma}i_d - \frac{1-\sigma}{\sigma}\left(\frac{i_d - i_\mu}{\tau_r}\right) + v_d \quad (3.25)$$

$$\frac{di_q}{dt} = -\frac{R_s}{L_s\sigma}i_q - \frac{1-\sigma}{\sigma\tau_r}i_q + v_q \quad (3.26)$$

$$\frac{di_\mu}{dt} = \frac{i_d - i_\mu}{\tau_r} \quad (3.27)$$

A state feedback controller has been developed for the above model. Furthermore, under the assumption that the nonlinearities removed from the original model can be compensated by the integral action, the controller has been tested for the system both with decoupling and without it.

As it can be seen in figure 3.10, both controllers present a similar performance in terms of convergence speed and overshoot. Furthermore, the control action is similar, which leads to the conclusion that the integral action is able to cope with the neglected nonlinearities. Furthermore, the nonlinearity cancellation is not well defined for $i_\mu = 0$, which pushes the linear controller with no nonlinearity cancellation as the chosen control option.

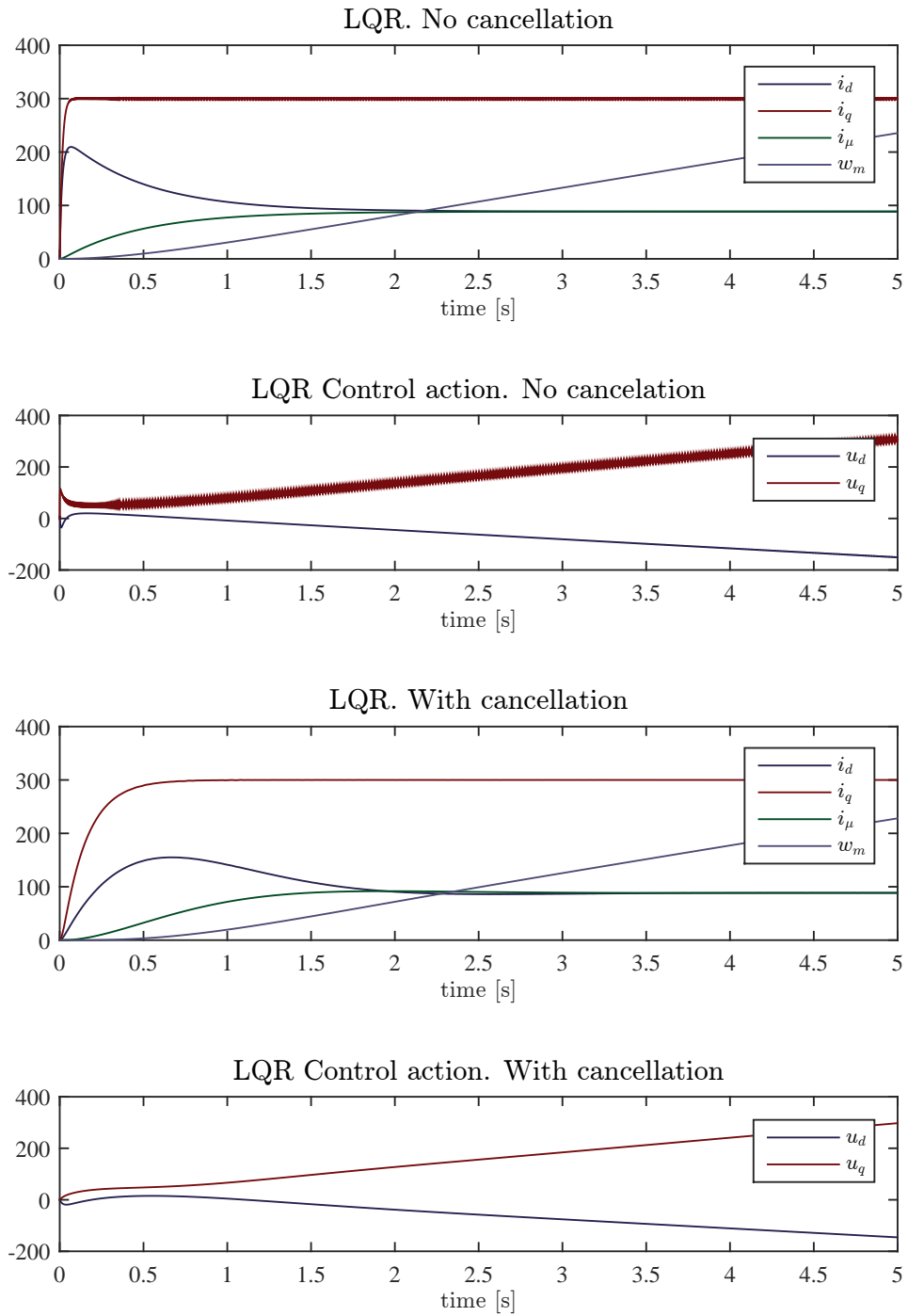


Figure 3.10: Performance of the LQR current controller, with and without using cancellation of non-linearities

3.2.8 State estimation

As already mentioned, only measurements of i_d and i_q are available. Therefore, i_μ must be estimated. In much of the literature where FOC is presented [1][13][23], an open loop estimation is proposed.

$$\hat{i}_\mu = \frac{i_d}{\frac{1}{\tau_r} + s} \quad (3.28)$$

Looking at equation (3.27) one can understand how this may work, as i_μ will converge towards i_d regardless of any deviation of τ_r from the actual value. Furthermore, in many of the schemes presented so far, i_μ is meant to remain constant, or vary slowly at most. As a matter of fact, it is not uncommon to find implementations where the estimate of i_μ is replaced by its "asymptotic certainty equivalent" (page 386 in [23]), i.e. the reference value of i_d . On a slightly different topic, this is the reason the second term in (3.25) is often neglected during control design in some of the literature (see section on decoupling in [13]).

A topic that in the author's view has a big impact on the estimation, and it is often neglected in the literature, is the estimation of the rotor field angle α_μ , which is needed for the transformation to dq-axis, and it is key for FOC. This angle is simply found by integration:

$$\dot{\hat{\alpha}}_\mu = \hat{\omega}_s = \omega_m + \frac{1}{\tau_r} \frac{i_q}{\hat{i}_\mu} \quad (3.29)$$

One may see that since i_q is found by means of $\hat{\alpha}_\mu$ in the rotation defined by (2.86), i_q turns out to be itself an estimate, which depends on $\hat{\alpha}_\mu$. Thus in open loop, an error in the estimation of any of the two variables will propagate, and will of course deteriorate the performance of the controller.

Despite the many concerns raised in [23] about the "separation principle" not holding for this specific case, observer design for flux estimation is a prolific topic as shown by the numerous existing publications, some examples are [11][25][12] and [5]. Consider now equations (3.19), (3.20), (3.21) and (3.29) as a model for estimation. With output:

$$\begin{bmatrix} i_\alpha \\ i_\beta \end{bmatrix} = \begin{bmatrix} \cos(\alpha_\mu) & \sin(\alpha_\mu) \\ -\sin(\alpha_\mu) & \cos(\alpha_\mu) \end{bmatrix}^{-1} \cdot \begin{bmatrix} i_d \\ i_q \end{bmatrix} \quad (3.30)$$

With ω_m available as a measurement. The presence of a singularity in $i_\mu = 0$ forces the designer to make use of heuristics to avoid instability of the filter close to the singularity. Furthermore, rotor flux angle α_μ cannot be estimated if (3.30) is not

included as part of the model. And when included, its sinusoidal nature makes estimation difficult.

A more suitable model is then required for estimation. Equations (2.101) - (2.104) in Section 2.7 are a description of the motor on dq axis rotating at an arbitrary speed ω_s . If an static reference frame is chosen, i.e. $\omega_s = 0$, the following model is obtained:

$$\frac{di_d}{dt} = \frac{1}{L_s\sigma}u_d - \left(\frac{R_s}{L_s\sigma} + \frac{1-\sigma}{\sigma\tau_r}\right)i_d + \frac{L_m}{\sigma L_s L_r \tau_r}\Psi_d + \frac{L_m}{\sigma L_s L_r}\omega_m\Psi_q \quad (3.31)$$

$$\frac{di_q}{dt} = \frac{1}{L_s\sigma}u_q - \left(\frac{R_s}{L_s\sigma} + \frac{1-\sigma}{\sigma\tau_r}\right)i_q - \frac{L_m}{\sigma L_s L_r}\omega_m\Psi_d + \frac{L_m}{\sigma L_s L_r \tau_r}\Psi_q \quad (3.32)$$

$$\frac{d\Psi_d}{dt} = \frac{L_m}{\tau_r}i_d - \frac{1}{\tau_r}\Psi_d - \omega_m\Psi_q \quad (3.33)$$

$$\frac{d\Psi_q}{dt} = \frac{L_m}{\tau_r}i_q + \omega_m\Psi_d - \frac{1}{\tau_r}\Psi_q \quad (3.34)$$

In order to build the EKF, the Jacobian of the system equations needs to be computed:

$$\mathbf{J} = \begin{bmatrix} -\left(\frac{R_s}{L_s\sigma} + \frac{1-\sigma}{\sigma\tau_r}\right) & 0 & \frac{L_m}{\sigma L_s L_r \tau_r} & \frac{L_m}{\sigma L_s L_r}\omega_m \\ 0 & -\left(\frac{R_s}{L_s\sigma} + \frac{1-\sigma}{\sigma\tau_r}\right) & -\frac{L_m}{\sigma L_s L_r}\omega_m & \frac{L_m}{\sigma L_s L_r \tau_r} \\ \frac{L_m}{\tau_r} & 0 & -\frac{1}{\tau_r} & -\omega_m \\ 0 & \frac{L_m}{dt} & \omega_m & -\frac{1}{\tau_r} \end{bmatrix} \quad (3.35)$$

As opposed to the rotor flux reference frame model, this one is well defined for all values. Furthermore, rotor flux angle can be computed as:

$$\hat{\alpha}_\mu = \arctan \frac{\hat{\Psi}_q}{\hat{\Psi}_d} \quad (3.36)$$

Since both Ψ_d and Ψ_q are observable, is possible to keep accurate track of α_μ , regardless of parameter deviation. Rotor current can be computed, as follows:

$$\hat{i}_\mu = \frac{\sqrt{\hat{\Psi}_d^2 + \hat{\Psi}_q^2}}{L_m} \quad (3.37)$$

It should also be noted that there is no need to measure the input voltage u_d and u_q , as it can be computed from as it is the same as the voltage reference introduced to the inverter. However, this must be considered during the tuning process. As was shown in section 2.5, the output voltage of the inverter is far from continuous, therefore the expected current will present a ripple. When tuning the EKF, this ripple has been considered as noise in the measurement. Furthermore, as the control input considered by the filter differs from the actual input to the system, the covariance for the states affected, i.e. i_d and i_q , has been set 10 times bigger than those of the

remaining two.

Figure 3.11 shows the performance of the filter. Because of the concerns in the literature on the robustness of the filter respect variations in the R_r parameter, the filter has been run for the same set of data with both the right value of R_r and with a deviation of 200%. To improve the prediction step, a 4th order Runge-Kutta (RK4)

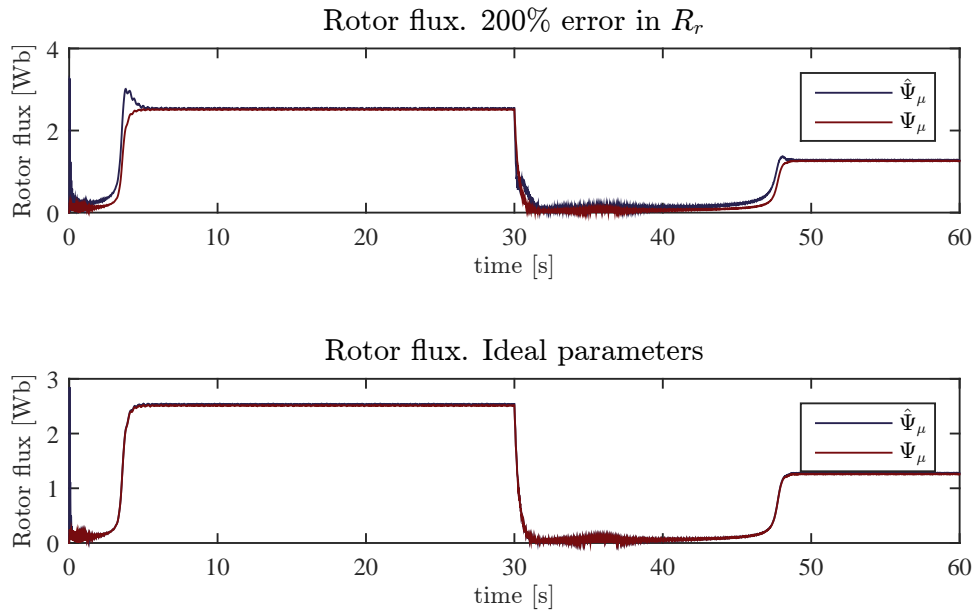


Figure 3.11: Estimation of the rotor flux with the right value of R_r and 200% off

algorithm has been used instead of the usual Euler integration. The following figure shows the performance of the filter using Euler's integration and RK4, and different time steps.

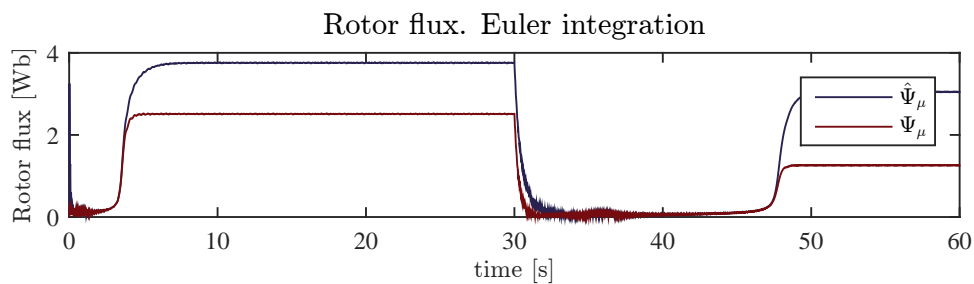


Figure 3.12: Estimation using a Euler integration and $100_{\mu s}$ sampling rate

3.2.9 Simulation results of the observer based controller of the motor

The performance of the controller is shown here. A speed loop has been built on top of the current loop. This loop gives computes the torque command, which is proportional to current i_q . Figure 3.13 shows the motor following the command.

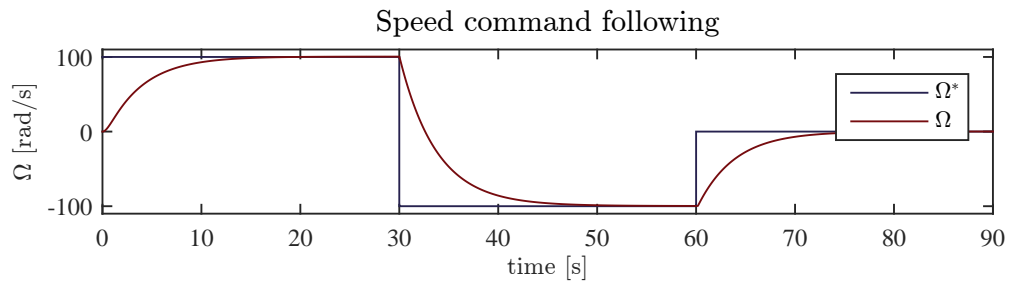


Figure 3.13: Motor speed following the reference

It is worth it to compare the behavior with that of the open loop in figure 2.26. Once taken care of the current, the only remaining dynamics are the mechanical dynamics. Figure 3.14 shows the response of the current when following a pulse

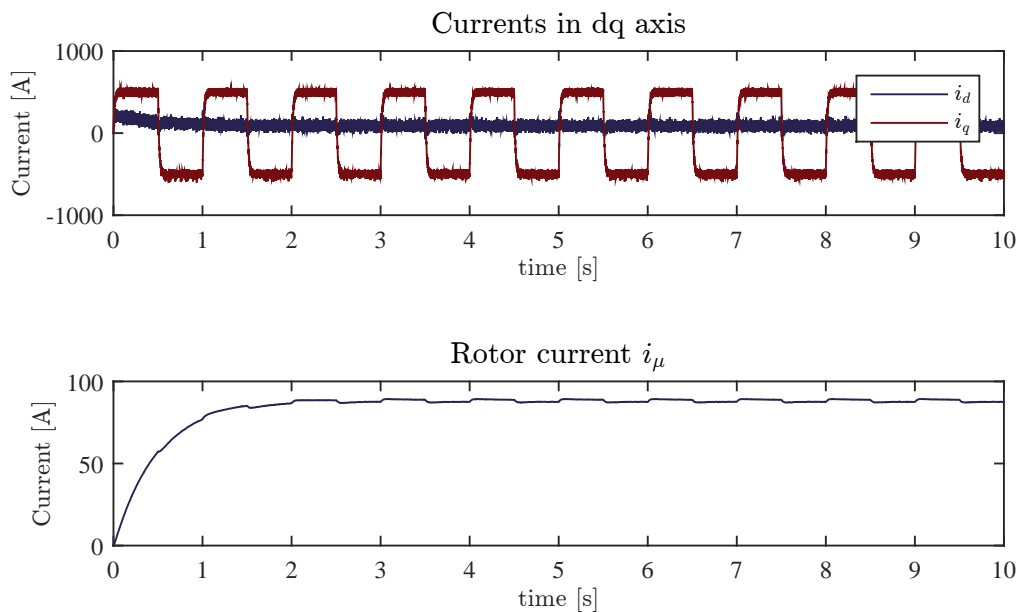


Figure 3.14: Insert Caption

train reference. Despite of the noisy measurements, the comman following is very

good. Furthermore, the rotor current, proportional to the rotor flux, reveals the effect of the cross-coupling between i_d and i_q . Because of the noisy data, the same effect can hardly be observed in i_d .

3.2.10 Performance of the classical control approach

Simulation results are shown for the whole system. The same speed command is given as in the previous case. Command following of the bus voltage, battery current, motor speed and i_q is shown in figure 3.15. In general, performance is good. Notice the notch the braking produces in the bus voltage. Also the jump in current in the battery. Figure 3.16 Shows a situation where the battery has low charge. This can be seen because of the fast descent of the battery voltage shown in the lower figure. The consequence of this is that the for the same power drawn from the battery, more current is need. However, the current is limited, and the bus voltage drops inexorably, until the bus collapses.

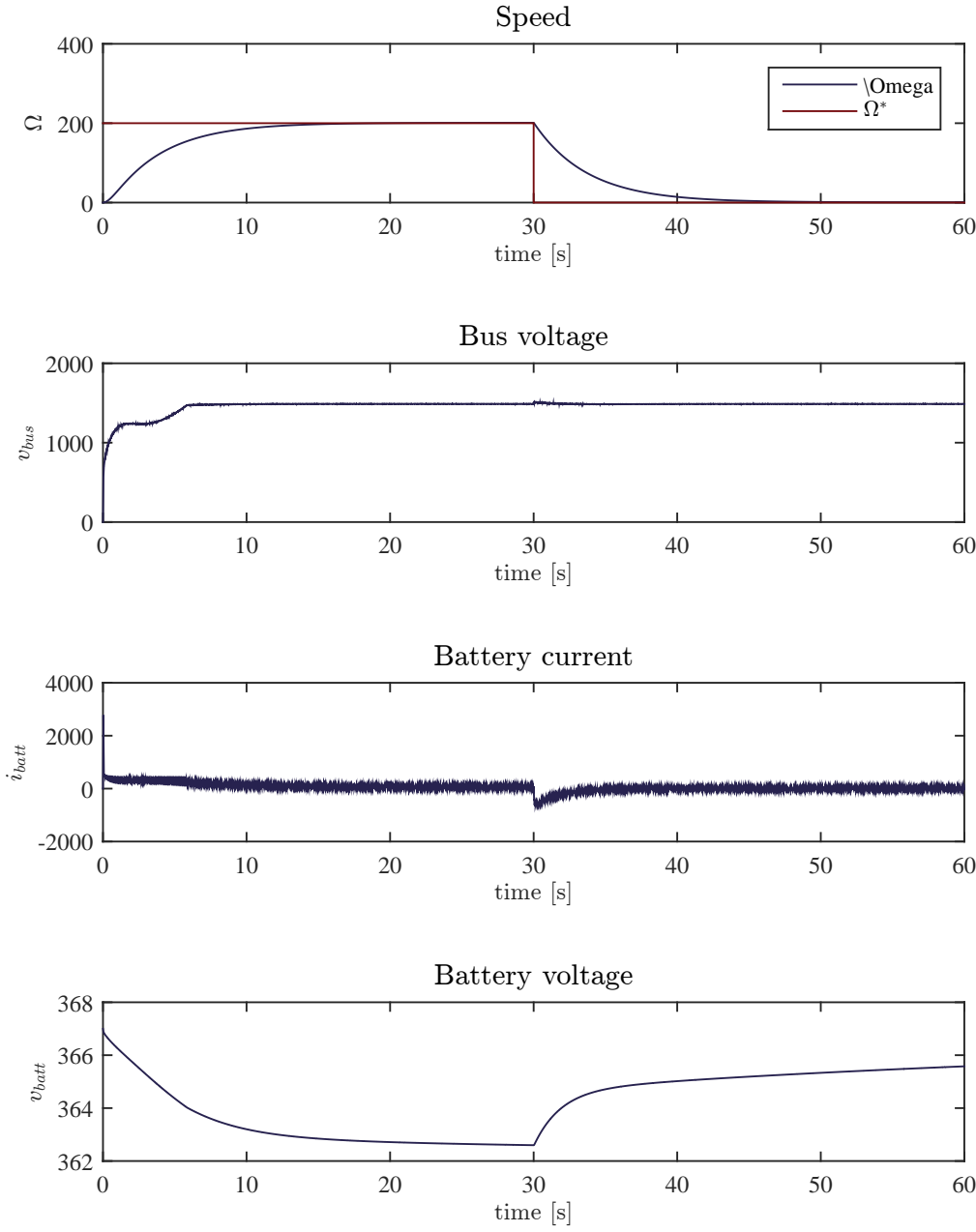


Figure 3.15: Normal operation

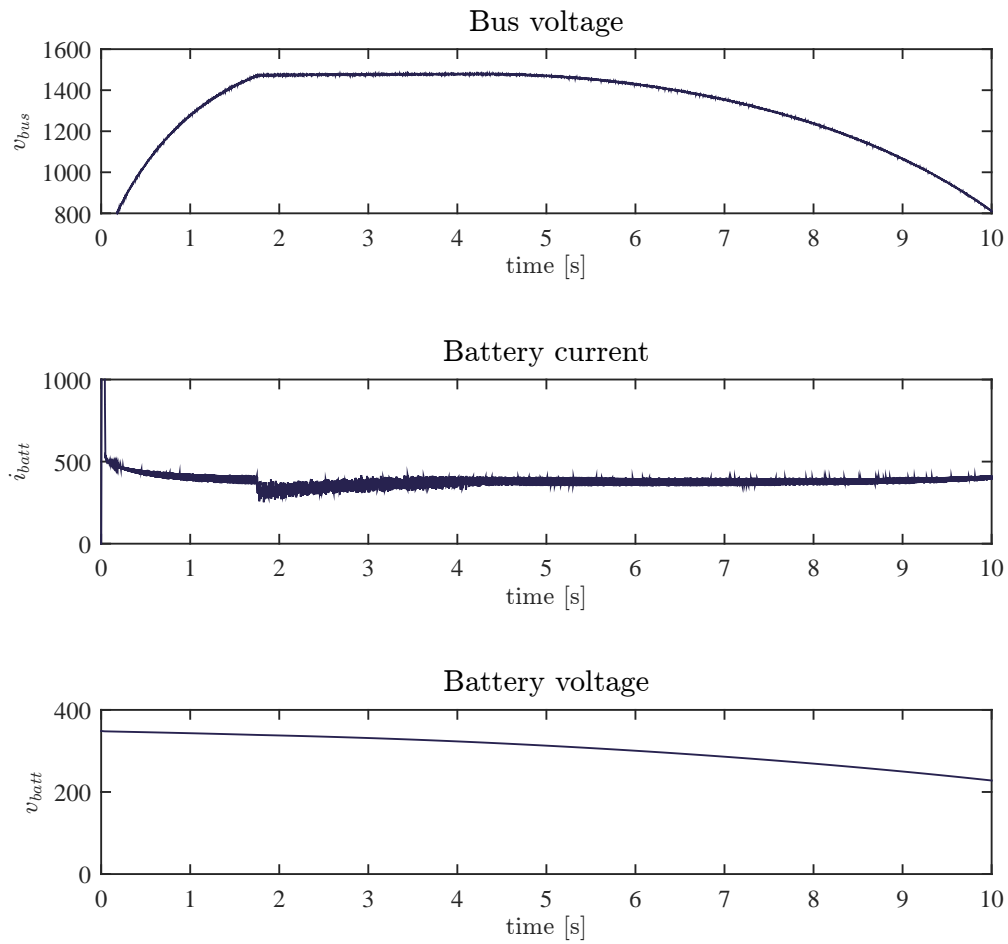


Figure 3.16: Operation at low SOC. The bus collapses, as the battery cannot meet the demand of current.

Chapter 4

Model Predictive Control

4.1 Model Predictive Control Approach

In Model Predictive Control, the optimal control input is found by solving online a constrained optimization problem. The problem is posed as follows for a discrete system:

$$\min_u \Psi(x_{k+N}) + \sum_{i=0}^{N-1} J(x_{k+i}, u_{k+i}) \quad (4.1a)$$

s.t.

$$x_{k+i+1} = f(x_{k+i}, u_{k+i}) \quad (4.1b)$$

$$x_{k+i} \in \mathcal{X} \quad (4.1c)$$

$$u_{k+i} \in \mathcal{U} \quad (4.1d)$$

$$x_{k+N} \in \mathcal{T} \quad (4.1e)$$

where:

$f(x_k, u_k)$ is the set of equations describing the system dynamics

\mathcal{X} is the set of all possible (constrained) states

\mathcal{U} is the set of all possible (constrained) inputs

\mathcal{T} is the set of all states so that if $x_k \in \mathcal{T}$, $x_{k+1} \in \mathcal{T}$

The solution to the above problem is the control input for the next N time instants. In this sense, the control input has been computed considering not only how the system will behave in the foreseeable future, as opposed to considering just the current state on traditional controllers. This foreseeable future is known as horizon. Furthermore, the problem considers the constraints imposed by the system and actuators and, if feasible, finds the optimal trajectory inside said constraints. Under the following assumptions, the solution to (4.1) stabilizes the system [9]:

A1: The terminal state satisfies the state constraints, i.e. $\mathcal{T} \subseteq \mathcal{X}$

A2: The control constraint is satisfied for x_{k+N} , i.e. $u \in \mathcal{U}, \forall x \in \mathcal{T}$

A3: Ψ is a local Lyapunov function, i.e. $\Psi(x, u) + J(x, u) \leq 0, \forall x \in \mathcal{T}$

The control input obtained by solving problem (4.1) as stated, will try to bring all the states to the origin. The problem can be modified to track a reference r by shifting the origin to a reference state x_r :

$$\min_u \Psi(x_{k+N} - x_r) + \sum_{i=0}^{N-1} J(x_{k+i} - x_r, u_{k+i} - u_r) \quad (4.2a)$$

s.t.

$$x_{k+i+1} = f(x_{k+i}, u_{k+i}) \quad (4.2b)$$

$$x_{k+i} \in \mathcal{X} \quad (4.2c)$$

$$u_{k+i} \in \mathcal{U} \quad (4.2d)$$

$$x_{k+N} \in \mathcal{T}(x_r) \quad (4.2e)$$

Where x_r and u_r can be found by solving:

$$\min_{x_r, u_r} u_r^T R u_r \quad (4.3a)$$

s.t.

$$f(x_r, u_r) = 0 \quad (4.3b)$$

$$h(x_r, u_r) = r \quad (4.3c)$$

$$u_{min} \leq u_r \leq u_{max} \quad (4.3d)$$

where:

$h(x_k, u_k)$ is a function mapping the states to the outputs of the system

u_{max} is the maximum input u_r

u_{min} is the minimum input u_r

So far nothing has been said about the nature of the system $f(x, u)$. Some results in non-linear model predictive control can be found in [34]. It is however for linear systems that most of the proofs and results can be found, as it can be seen in [9]. In the sequel the work will be restricted to linear systems.

In this section an MPC for the system described in the 2 is presented. First a linear model of the system is obtained, then the system constraints are set. Because of the computational load of solving an optimization problem, the sampling time cannot be very fast. For a given horizon, the smaller the sampling time, the more variables and the more computationally intensive the problem becomes. Furthermore, the horizon has to be long enough to cover a whole transient to be effective.

In an effort to keep the problem simple, and allow slow sampling time, the current for the battery and motor are controlled independently. Therefore the problem reduces to finding the references for said loops. The controllers are the same as those presented in sections 3.2.4 and 3.2.6.

4.2 MPC model

Problem (4.3) will be used to obtain the optimal control for a linear system:

$$x_{k+1} = Ax_k + Bu_k \quad (4.4)$$

$$y_k = Cx_k + Du_k \quad (4.5)$$

The variables chosen as states are:

$$x = \begin{bmatrix} v_{c_1} \\ v_{c_2} \\ soc \\ v_d \\ \Omega \end{bmatrix} \quad (4.6)$$

where:

| | | |
|-----------|---|-------------------|
| v_{c_n} | is the voltage of the n RC circuit of the battery | [V] |
| soc | is the state of charge of the battery | [.] |
| v_d | is the bus voltage | [V] |
| Ω | is the mechanical speed of the motor | $[\frac{rad}{s}]$ |

It has already been said that the control inputs to the system are the current references of the battery and the motor:

$$u = \begin{bmatrix} i_{batt} \\ i_q \end{bmatrix} \quad (4.7)$$

Here, i_q is equivalent to the torque reference. The dynamic equations for the battery have already been described in section 2.2 in 2, and are repeated here:

$$\frac{dv_{c_1}}{dt} = -\frac{1}{\tau_1}v_{c_1} - \frac{1}{C_1}i_{batt} \quad (4.8)$$

$$\frac{dv_{c_2}}{dt} = -\frac{1}{\tau_2}v_{c_2} - \frac{1}{C_2}i_{batt} \quad (4.9)$$

$$\frac{dSoC}{dt} = -\frac{1}{C} \quad (4.10)$$

The model of the DC-DC converter is omitted because of its fast dynamics. Only the energy transfer from the bus to the battery and from the bus to the motor has been

considered. The energy stored in the capacitor is:

$$E_{bus}(t) = \frac{1}{2}Cv_{bus}^2(t) = \int_0^t P_{batt}(t) - P_m(t)dt \quad (4.11)$$

where:

| | | |
|------------|---|-----|
| C | is the capacitance of the bus capacitor | [F] |
| P_{batt} | is the power poured into the bus from the battery | [W] |
| P_m | is the power drawn from bus by the motor | [W] |

Furthermore:

$$P_{batt}(t) = v_{batt}(t) \cdot i_{batt}(t) \quad (4.12)$$

$$P_m(t) = 3/2 \cdot \text{Re}(v_s(t) \cdot i_s^*(t)) \quad (4.13)$$

where:

| | | |
|------------|-----------------------------|-----|
| v_{batt} | is the battery voltage | [V] |
| v_s | is the stator voltage in dq | [V] |
| i_s | is the stator current in dq | [W] |

The voltage balance equation for the bus can then be obtained by taking the time derivative of (4.11):

$$\frac{dv_{bus}}{dt} = \frac{P_{batt}(t)}{Cv_{bus}(t)} - \frac{P_m(t)}{Cv_{bus}(t)} \quad (4.14)$$

The first term in the above equation can be simplified by expanding it and making a few assumptions:

$$\frac{P_{batt}(t)}{Cv_{bus}(t)} = \frac{v_{batt}(t) \cdot i_{batt}(t)}{Cv_{bus}(t)} \quad (4.15)$$

To minimize ripple in the battery current i_{batt} , the duty ratio should be kept as close to $d \approx 0.5$ as possible. As a result $v_{bus}(t) \approx 2v_{batt}(t)$. Then the above expression reduces to:

$$\frac{P_{batt}(t)}{v_{bus}(t)} = \frac{i_{batt}(t)}{2C} \quad (4.16)$$

Obtaining a linear expression for $\frac{P_m(t)}{Cv_{bus}(t)}$ is less straight forward. Starting with the definition of electrical power [13] for the motor:

$$P_m(t) = \frac{3}{2} \cdot \text{Re}(v_s(t) \cdot i_s^*(t)) \quad (4.17)$$

$$= \frac{3}{2} \cdot \text{Re}((u_d(t) + ju_q(t)) \cdot (i_d(t) - ji_q(t))) \quad (4.18)$$

$$= \frac{3}{2} (u_d(t)i_d(t) + u_q(t)i_q(t)) \quad (4.19)$$

Where i_d is kept constant by the motor current controller, and i_q is an input of the MPC model. Furthermore, their dynamics are faster than the sampling rate of the MPC controller and consequently they set between sampling instants. Then it is reasonable to assume that they are exactly equal to their respective reference values. Voltages u_d and u_q can then be found by setting the time derivatives to zero in (3.19) - (3.21) and solving for u_d and u_q :

$$u_d = -L_s \sigma \omega_m i_q - \frac{L_s \sigma}{i_\mu \tau_r} i_q^2 \quad (4.20)$$

$$u_q = \frac{L_s}{\tau_r} i_q + L_s i_\mu \omega_m \quad (4.21)$$

Introducing this result back in (4.19), an expression for the power is found:

$$P_m = \frac{3}{2} \left((1 - \sigma) \frac{L_s}{\tau_r} i_q^2 + (1 - \sigma) L_s i_\mu i_q \omega_m \right) \quad (4.22)$$

Before introducing it in (4.14), the expression needs to be linearized:

$$\frac{P_m}{C v_{bus}} = \frac{3}{2C} \left((1 - \sigma) \frac{L_s}{\tau_r} \frac{i_q^2}{v_{bus}} + (1 - \sigma) L_s \frac{i_\mu i_q \omega_m}{v_{bus}} \right) \quad (4.23)$$

Choosing an operating point:

$$i_q = i_{q0} \quad (4.24)$$

$$\omega_m = \omega_{m0} \quad (4.25)$$

$$v_{bus} = v_{bus0} \quad (4.26)$$

$$i_\mu = \frac{1}{L_m} \quad (4.27)$$

The expression is linearized for i_d , ω_m and v_{bus} :

$$\begin{aligned} \frac{P_m}{C v_{bus}} = \frac{3}{2C} \left(\frac{(1 - \sigma) L_s}{v_{bus0}} \left(\frac{2i_{q0}}{\tau_r} + \frac{\omega_{m0}}{L_m} \right) i_q + (1 - \sigma) \frac{L_s i_{q0}}{L_m v_{bus0}} \omega_m \right. \\ \left. - \frac{(1 - \sigma) L_s}{v_{bus0}^2} \left(\frac{i_{q0}^2}{\tau_r} + \frac{i_{q0} \omega_{m0}}{L_m} \right) v_{bus} \right) \end{aligned}$$

Only the mechanical dynamics equation is left:

$$\frac{d\Omega}{dt} = -\frac{1}{J} \Omega - \frac{K}{J} \Omega + \frac{3}{2} \frac{L_m}{L_r} p i_q \quad (4.28)$$

where:

| | | |
|-----|---------------------------------|-----------------|
| J | is the moment of inertia | $[N \cdot m^2]$ |
| p | is the number of pairs of poles | $[.]$ |

Then the system in matrix form can be stated as follows:

$$A = \begin{bmatrix} -\frac{T_s}{\tau_1} & 0 & 0 & 0 & 0 \\ 0 & -\frac{T_s}{\tau_1} & 0 & 0 & 0 \\ 0 & 0 & 1 & 0 & 0 \\ 0 & 0 & 0 & -aT_s & -b \\ 0 & 0 & 0 & 0 & -\frac{KT_s}{J} \end{bmatrix} \quad (4.29)$$

where T_s is the time step and:

$$a = -\frac{3(1-\sigma)L_s}{2Cv_{bus0}^2} \left(\frac{i_{q0}^2}{\tau_r} + \frac{i_{q0}\omega_{m0}}{L_m} \right) \quad (4.30)$$

$$b = \frac{3}{2}(1-\sigma) \frac{L_s i_{q0}}{L_m C v_{bus0}} \quad (4.31)$$

Furthermore the input matrix B is:

$$B = \begin{bmatrix} -\frac{T_s}{C_1} & 0 \\ -\frac{T_s}{C_2} & 0 \\ -\frac{T_s}{C_{As}} & 0 \\ \frac{T_s}{2C} & -c \\ 0 & \frac{3}{2} \frac{L_m}{L_r} \rho T_s \end{bmatrix} \quad (4.32)$$

where:

$$c = \frac{3(1-\sigma)L_s}{2Cv_{bus0}} \left(\frac{2i_{q0}}{\tau_r} + \frac{\omega_{m0}}{L_m} \right) \quad (4.33)$$

4.3 State and input constraints

In the previous section linear dynamics of the system have been defined. Additional constraints are imposed to the states and inputs. These are derived from the system specifications of the different components of the system.

4.3.1 Constraints imposed by the battery

There is a maximum and a minimum voltage the battery may attain, as well as maximum and minimum charge capacity:

$$v_{b_{min}} \leq v_{c_1} + v_{c_2} + k \cdot soc + v_{offset} \leq v_{b_{max}} \quad (4.34)$$

$$soc_{min} \leq soc \leq soc_{max} \quad (4.35)$$

where:

| | | |
|---------------|---|-----|
| $v_{b_{min}}$ | is the minimum allowed voltage of the battery | [V] |
| $v_{b_{max}}$ | is the maximum allowed voltage of the battery | [V] |
| k | is the slope of the linear approximation of the OCV | [V] |
| v_{offset} | is the offset voltage of said approximation | [V] |

Finally, constraints for the battery charging and discharging current can be chosen based on manufacturer specifications:

$$-i_{dsch} \leq i_b \leq i_{ch} \quad (4.36)$$

where:

| | | |
|------------|------------------------------------|-----|
| i_{dsch} | is the maximum discharging current | [A] |
| i_{ch} | is the maximum charging current | [A] |

4.3.2 Constraints imposed by the DC-DC converter

There also exists a hardware limitation on the duty ratio that the DC-DC converter can achieve, and therefore on the voltage ratio between the battery and the bus voltage. Furthermore, it is desirable that ratio is as closed to 2 as possible. Therefore two additional constraints are defined:

$$v_{d_{min}} \leq v_d \leq v_{d_{max}} \quad (4.37)$$

$$v_d = 2 \cdot (v_{c_1} + v_{c_2} + k \cdot soc + v_{offset}) \quad (4.38)$$

This last constraint, relating the battery voltage and the bus voltage is very restrictive as it is. To minimize this restriction an additional variable ϵ_d is introduced:

$$|v_d - 2 \cdot (v_{c_1} + v_{c_2} + k \cdot soc + v_{offset})| \leq \epsilon_d \quad (4.39)$$

Then ϵ_d serves as a free variable, that will be minimized together with the rest of the variables, while allowing for some discrepancy in the original equality constraint. The higher the corresponding weight in the objective, the lower the discrepancy, and vice versa.

4.3.3 Constraints imposed by the induction motor

By nameplate data, there is a maximum current i_{max} at which the motor may operate in a continuous manner. This limits current i_q as follows:

$$i_{max}^2 \leq \frac{3}{2} (i_d^2 + i_q^2) \quad (4.40)$$

Since i_d is kept constant by the controller, the boundary of i_q can easily be found. Furthermore, the steady state behavior impose constraints on the torque. Since the

torque is proportional to i_q , the limit can be found by analyzing (3.20) in steady state:

$$i_q = \frac{\tau_r}{L_s} u_q - \frac{\tau_r}{L_m} p \Omega \quad (4.41)$$

The maximum achievable voltage u_q is:

$$|u_q| \leq \frac{2}{3\sqrt{3}} v_d \quad (4.42)$$

Therefore the constraint can be written as function of two of the states:

$$-\frac{2}{3\sqrt{3}} \frac{\tau_r}{L_s} v_d - \frac{\tau_r}{L_m} p \Omega \leq i_q \leq \frac{2}{3\sqrt{3}} \frac{\tau_r}{L_s} v_d - \frac{\tau_r}{L_m} p \Omega \quad (4.43)$$

It turns out that in the case at hand the lower bound defined by the constraint in (4.40) is more restrictive than the one defined in the left-hand side of (4.43), and can be ignored.

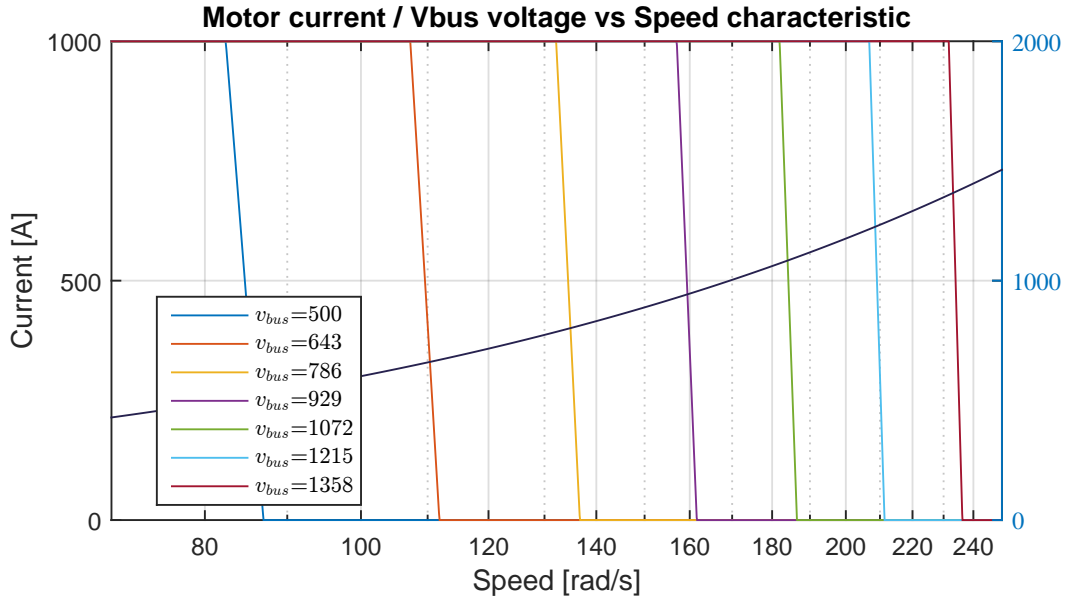


Figure 4.1: Current (Torque) speed of the motor. Crossed by Voltage speed characteristic. Notice this is logarithmic scale.

Furthermore, constraint (4.43) defines a very steep relation between i_q and Ω . This allows to transform it into an state constraint as follows:

$$\Omega \leq \frac{2}{3\sqrt{3}} \frac{L_m}{L_s} v_d - \frac{L_m}{p\tau_r} i_{q_{max}} \quad (4.44)$$

This can be interpreted as the maximum speed that can be achieved for a given bus voltage v_d . Both constraints are shown in the figure above. Notice the mentioned steep descent of the voltage close before the maximum achievable speed defined by (4.44).

4.3.4 Summary of the constraints

The constraints are now set in a way that they are easy to deal with. Starting with the state inequality constraints, they are introduced as:

$$g_{lim^-} \leq Gx_{k+i} \leq g_{lim^+} \quad (4.45)$$

where G is:

$$G = \begin{bmatrix} 1 & 1 & k & 0 & 0 \\ 0 & 0 & 1 & 0 & 0 \\ 0 & 0 & 0 & 1 & 0 \\ 0 & 0 & 0 & \frac{2}{3\sqrt{3}}\frac{L_m}{L_s} & -\Omega \end{bmatrix} \quad (4.46)$$

The limits g_{lim^+} and g_{lim^-} are:

$$g_{lim^+} = \begin{bmatrix} v_{b_{max}} \\ SOC_{max} \\ v_{d_{max}} \\ v_{d_{max}} \end{bmatrix} \quad g_{lim^-} = \begin{bmatrix} v_{b_{min}} \\ SOC_{min} \\ v_{d_{min}} \\ \frac{L_m}{p\tau_r} i_{q_{max}} \end{bmatrix} \quad (4.47)$$

A single equality constraint exist. It is rewritten here in matrix form for consistency:

$$Dx_{k+i} + \epsilon_{d_{k+i}} = d \quad (4.48)$$

where D is:

$$D = \begin{bmatrix} -2 & -2 & -2k & 1 & 0 \end{bmatrix} \quad (4.49)$$

and d :

$$d = -2v_{offset} \quad (4.50)$$

The input constraints can be written as:

$$u_{lim^-} \leq u \leq u_{lim^+} \quad (4.51)$$

with:

$$u_{lim^+} = \begin{bmatrix} i_{dsch} \\ i_{q_{max}} \end{bmatrix} \quad u_{lim^-} = \begin{bmatrix} -i_{ch} \\ -i_{q_{max}} \end{bmatrix} \quad (4.52)$$

4.3.5 Objective function

The objective function measures the performance of the controller. Hence the objective function should capture the goals of the controller. In most cases, this included, the main goal is to reach the reference with the minimum effort, i.e. minimizing the control input. Furthermore, losses in the motor and battery should be minimized as well, and therefore will be included in the objective.

The MPC problem is posed as a convex problem. Quadratic forms are then chosen for the objective. This is not only convenient on its convexity, but also because power losses can be expressed in quadratic terms. This knowledge can be used to define the objective.

$$J(x, u) = x_{k+N}^T S x_{k+N} + \sum_{i=0}^{N-1} x_{k+i}^T Q x_{k+i} + u_{k+i}^T R u_{k+i} + \epsilon_{k+i}^T E \epsilon_{k+i} \quad (4.53)$$

where:

$$\begin{aligned} Q &\geq 0 \\ R &\geq 0 \end{aligned}$$

Appropriate values for Q and R can be found from the system characteristics. Q will be derived from the states, starting with v_{C_n} , losses P_{R_n} on the parallel resistor R_n can be described as function of the state itself:

$$P_{R_n} = \frac{v_{C_n}^2}{R_n} \quad (4.54)$$

Furthermore, losses due to mechanical friction P_Ω can be described as:

$$P_\Omega = K\Omega^2 \quad (4.55)$$

The remaining two states have no impact on the power efficiency nor are required to attain low values, therefore, their weights can be chosen arbitrarily small as long as Q remains positive definite. This yields the following Q matrix:

$$Q = \begin{bmatrix} \frac{1}{R_1^2} & 0 & 0 & 0 & 0 \\ 0 & \frac{1}{R_2} & 0 & 0 & 0 \\ 0 & 0 & q_{soc} & 0 & 0 \\ 0 & 0 & 0 & q_{bus} & 0 \\ 0 & 0 & 0 & 0 & K \end{bmatrix} \quad (4.56)$$

As for the inputs, i_q can be related to the losses in the motor's stator as follows:

$$P_s = i_q^2 R_s \quad (4.57)$$

Furthermore, an additional weight can be set to penalize excessive input by using the maximum allowed current as follows:

$$r_s = \frac{1}{i_{max}^2} \quad (4.58)$$

Corresponding weights for i_{batt} can be chosen in the same way:

$$r_{batt} = \frac{1}{i_{dsch}^2} \quad (4.59)$$

Hence R is:

$$R = \begin{bmatrix} \frac{R_s i_{max}^2 + 1}{i_{max}^2} & 0 \\ 0 & \frac{1}{i_{dsch}^2} \end{bmatrix} \quad (4.60)$$

4.3.6 Reference tracking

In this section the original problem is modified to allow reference tracking. Starting with problem (4.2):

$$\min_u \quad (x_{k+N} - x_r)^T P (x_{k+N} - x_r) + \sum_{i=0}^{N-1} (x_{k+i} - x_r)^T Q (x_{k+i} - x_r) + u_{k+i}^T R (u_{k+i} - u_r) \quad (4.61a)$$

s.t.

$$x_{k+i+1} = Ax_{k+i} + Bu_{k+i} \quad (4.61b)$$

$$d = Dx_{k+i} + \epsilon_{d_{k+i}} \quad (4.61c)$$

$$g_{lim-} \leq Gx_{k+i} \leq g_{lim+} \quad (4.61d)$$

$$u_{lim-} \leq u \leq u_{lim+} \quad (4.61e)$$

Furthermore, problem (4.3) needs to be solved to find the references:

$$\min_{x_r, u_r} \quad u_r^T R u_r \quad (4.62a)$$

s.t.

$$\begin{bmatrix} A - I & B \\ C & 0 \end{bmatrix} \begin{bmatrix} x_r \\ u_r \end{bmatrix} = \begin{bmatrix} 0 \\ r \end{bmatrix} \quad (4.62b)$$

$$u_{min} \leq u_r \leq u_{max} \quad (4.62c)$$

Fortunately, the solution to the above problem can be written as a linear mapping from the reference to the states and control input:

$$\begin{bmatrix} x_r \\ u_r \end{bmatrix} = \begin{bmatrix} \Pi_x \\ \Pi_u \end{bmatrix} r \quad (4.63)$$

Feasibility can be increased by introducing an artificial reference as variable [8][6], and then penalizing its deviation from the original. Let the artificial reference be r_s , then the reference state and inputs are x_s and u_s . The final form of the problem is now stated:

$$\min_u J_k \quad (4.64a)$$

s.t.

$$x_{k+i+1} = Ax_{k+i} + Bu_{k+i} \quad (4.64b)$$

$$d = Dx_{k+i} + \epsilon_{d_{k+i}} \quad (4.64c)$$

$$g_{lim-} \leq Gx_{k+i} \leq g_{lim+} \quad (4.64d)$$

$$u_{lim-} \leq u \leq u_{lim+} \quad (4.64e)$$

$$x_s = \Pi_x r_s \quad (4.64f)$$

$$u_s = \Pi_u r_s \quad (4.64g)$$

where J_k is:

$$\begin{aligned} J_k = & (x_{k+N} - x_s)^T P (x_{k+N} - x_s) + (r - r_s)^T W (r - r_s) \\ & + \sum_{i=0}^{N-1} (x_{k+i} - x_s)^T Q (x_{k+i} - x_s) + (u_{k+i} - u_s)^T R (u_{k+i} - u_s) \end{aligned} \quad (4.65)$$

4.4 Conclusion

Unfortunately, the few results that had been obtained for this chapter cannot be shown. Regardless, some lessons can be learned by the set up of the problem alone, as has been exposed in this section. The first is that when trying to apply MPC on a complex system, a way must be found so the system is as linear as possible. The usual linearization techniques not always yields good results. This can be seen from the development of equations 4.14 and on. Keeping the system as energy level, while leaving dynamics to hierarchically lower controllers is probably the smartest way to apply MPC to a system like this. Finally, still on the topic of MPC, the introduction of a reference while retaining all the stability properties is a difficult topic, but also an interesting research area that should see more development.

The last conclusion on this specific chapter, but perhaps the most general of all, is that version control is important. Specially when working on topics for the first time. Mistakes are made and solutions are not always easy to find.... but making a copy of the version that works ('or sort of works') can save many wake nights. One should have known by now... but that is a topic for another report.

Chapter 5

Conclusion

Regretfully, very little can be obtained of the thesis as the work is not finished. If any, a summary of the work done, and some of the acquired knowledge.

The thesis has covered quite thoroughly, although under certain assumptions, the modeling of the traction set of a tram. A model of the battery pack has been developed, not before analyzing the extensive existing literature. Furthermore, modeling of power converters have been covered as well, explaining the theory behind a powerful tool such as the Generalized Average Models. The model for the well known induction motor has been reviewed. Not only that, but the thesis has made intensive use of the rotating frame and space vector theory in order to achieve control of the motor. Relevant in this same topic, is also the way the EKF has been build, to bring observability to a model where it wasn't obvious. Furthermore, this happens to be through a series of nonlinear transformation and within a very noisy context. Finally the whole control system has been evaluated, tested and reviewed.

The sad point to make, is the lack of the MPC that was the focus of the thesis. This leaves the reader, and the author, without the opportunity to being able to compare how both control perform. It may well be this is the reason the industry never really decided to step into modern control theory.

With this bittersweet (more bitter, than sweet) after taste, it has been though, revealing. The limitations of linear systems at some point, compared to its power at some other, make for an interesting topic. When dealing with the motor, for instance, the first attempt to control it was via linearization, which leads to how to choose the operating point without including the speed of the motor in it. This frustrating procedure, leads later to surprise when just removing the ugly terms out of the equation and adding integral action turns into success. Same happened when dealing with the MPC, this time with the lesson learned: try to look at it smart.

Results weren't perfect, but satisfactory enough. Wondering into the documentation available for MPC, one realizes that is because by limiting oneself to linear systems, that things such as ensuring feasibility and stability are possible. And despite all their limitation, they work, with the due care, as representations of non-linear systems.

Once again, a final off-topic remark. Cato the Elder used to finish his speeches by saying: "Ceterum censeo Carthaginem esse delendam", which revealed his obsession with the destruction of Carthage as a necessity for Rome. The author has now claimed on of such obsessions form himself, and coined a sentence for himself: "Furthermore, I consider that server side version must be updated regularly".

To the reader: The most sincere thanks from the author, for taking the time and the dedication to read this thesis. That despite the outcome, it has been a pleasure to write, and to feel free to wonder into any corner curiosity guided.

Bibliography

- [1] M. Ahmad. *High Performance AC Drives*. Ed. by Springer London Dordrecht Heidelberg New York. Springer, 2010.
- [2] Branko Blanusa Branko L. Dokic. *Power electronics: Converters and regulators*. Ed. by Springer Cham Heidelberg New York Dordrecht London. Springer, 2015.
- [3] Xue Li Wen Chen-George Yin Jiuchun Jiang Caiping Zhang Le Yi Wang. “Robust and Adaptive Estimation of State of Charge for Lithium-Ion Batteries”. In: *Transactions on Industrial Electronics* (2015).
- [4] Stefan Stumpp Michael A. Danzer Clemens Guenther Joaquim Klee Barillas. “A Dynamic Battery Model for Simulation of Battery-to-grid Applications”. In: *Innovative Smart Grid Technologies Europe 3* (2012), pp. 1–5.
- [5] Frede Blaabjerg Cristian Lascu Ion Boldea. “A class of speed-sensorless sliding mode observers for high-performance induction motor drives”. In: *Transactions on industrial electronics* 56 (2009), pp. 3394–3404.
- [6] T. Alamo E.F. Camacho D. Limon I. Alvarado. “MPC for tracking piecewise constant rreference for constrained linear systems”. In: *Automatica* 44 (2008), pp. 2382–2387.
- [7] Qingxi Hu Daizhan Cheng Yahong Zhu. “Stabilization of Switched Systems via Common Lyapunov Function”. In: *Proceedings of the 6th World Congress on Intelligent Control and Automation*. 2006.
- [8] Torkel Glad Daniel Simon Johan Lofberg. “Reference Tracking MPC using Terminal Set Scaling”. In: *51st IEEE Conference on Decision and Control*. 2012.
- [9] C.V. Rao P.O.M. Scokaert D.Q. Mayne J.B. Rawlings. “Constrained model predictive control: Stability and optimality”. In: *Automatica* 36 (2000), pp. 789–814.
- [10] A. Benchaib E. Prempain I. Postlethwaite. “A linear parameter variant H-infinity control design for an induction motor”. In: *Control Engineering Practice* 10 (2002), pp. 633–644.

- [11] A. Razek G. Garcia Soto E. Mendes. “Reduced-order observers for rotor flux, rotor resistance and speed estimation for vector control induction motor drives using the extended Kalman filter technique”. In: *Proceedings Electric Power Applications* 146 (1999), pp. 282–288.
- [12] Seth R. Sanders George C. Veeghese. “Observers for Flux Estimation in Induction Machines”. In: *Transaction on industrial electronics* 35 (1988), pp. 85–95.
- [13] Dieter Gerling. *Electrical Machines - Mathematical Fundamentals of Machine Topologies*. Ed. by Springer Heidelberg New York Dordrecht London. Springer, 2015.
- [14] J.H. Park S.W. Cha G.Y. Cho J.W. Choi. “Transient modeling and validation of lithium ion battery pack with air cooled thermal management system for electric vehicles”. In: *International Journal of Automotive Technology* 15 (2014), pp. 795–803.
- [15] Michael S. Mazzola Jianwei Li. “Accurate battery pack modeling for automotive applications”. In: *Journal of Power Sources* 237 (2013), pp. 215–228.
- [16] Huihuan Qian Tangsheng Xu Jingyu Yan Guoqing Xu. “Robust State of Charge Estimation for Hybrid Electric Vehicle: Framework and Algorithms”. In: *Energies* 3 (2010), pp. 1654–1672.
- [17] Christopher Lyness Nigel Taylor James Marco Kotub Uddin Alessandro Picarelli. “An Acausal Li-Ion Battery Pack Model for Automotive Applications”. In: *Energies* 7 (2014), pp. 5675–5700.
- [18] Bor Yann Liaw Matthieu Dubarry Nicolas Viullaume. “From Li-Ion single cell model to battery pack simu”. In: *International Conference on Control Applications* 17 (2008), pp. 708–713.
- [19] Dirk Uwe Sauer Michael A. Roscher. “Dynamic electric behavior and open-circuit-voltage modeling of LiFePO₄-based lithium ion secondary batteries”. In: *Journal of Power Sources* 196 (2011), pp. 331–336.
- [20] William P. Robbins Ned Mohan Tore M. Undeland. *Power electronics: Converters, applications and design*. Ed. by Bill Zobrist. John Wiley & Sons, 2003.
- [21] Francisco J. Maseda Oscar Barambones Aitor J. Garrido. “A Robust Field Oriented Control of Induction Motor with Flux Observer and Speed Adaptation”. In: *Emerging Technologies and Factory Automation*. 2003.
- [22] Hans-Peter Beck Meina Jiang Detlef Ohms Gunter Schaedlich Ralf Benger Heinz Wenzl. “Electrochemical and thermal modeling of lithium-ion cells for use in HEV or EV application”. In: *World Electric Vehicle Journal* 3 (2009), pp. 1–10.

- [23] Per Johan Nicklasson Herbertt Sira-Ramirez Romero Ortega Antonio Loria. *Passivity-based Control of Euler-Lagrange Systems: Mechanical, Electrical and Electromechanical Applications*. Ed. by Springer Verlag London. Springer, 1998.
- [24] Philip T. Krein Ryan C. Kroeze. “Electrical Battery Model for Use in Dynamic Electric Vehicle Simulations”. In: *Power Electronics Specialists Conference 2008 (2008)*, pp. 1336–1342.
- [25] M. Same Fadali Saeed Jafarzadeh Cristian Lascu. “State estimation of induction motor drives design Uncensored Kalman Filter”. In: *Transactions on industrial electronics* 59 (2012), pp. 4207–4217.
- [26] Ralph E. White Saeed Khaleghi Rahimian Sean Rayman. “Extension of physics-based single particle model for higher charge-discharge rates”. In: *Journal of Power Sources* 224 (2013), pp. 180–194.
- [27] Antoneta Iuliana Bratcu Seddik Bacha Iulian Munteanu. *Power Electronics Converters Modeling and Control*. Ed. by A. Johnson Michael J. Grimbale Michael. Springer, 2014.
- [28] several. *Dynamic and control of switched electronics systems*. Ed. by Luigi Ianneli Francesco Vasca. Springer, 2012.
- [29] Premanand Ramadass Ralph E. White Shriram Santhanagopalan Qingzhi Guo. “Review of mmodel for predicting the cycling performance of lithium ion batteries”. In: *Journal of Power Sources* 156 (2006), pp. 620–628.
- [30] Ulf Jonsson Stefan Almer. “Harmonic analysis of pulse-width modulated systems”. In: *Automatica* 45 (2009), pp. 851–862.
- [31] Javier Gazzari Robyn Jackey Tarum Huria Massimo Ceraolo. “High Fidelity Electrical Model with Thermal Dependence for Characterization and Simulation of High Power Lithium Battery Cells”. In: *Electrical Vehicle Conference - (2012)*, pp. 1–8.
- [32] Various. *Induction Motors - ModeModel and Control*. Ed. by Rui Esteves Araujo. InTech, 2012.
- [33] S.N. Vukosavic. *Electrical Machines*. Ed. by Springerlink. Springer Science, 2013.
- [34] S. Han W.H. Kwon. *Receding Horizon Control*. Ed. by Michael A. Jonhson Michael J. Grimbale. Springer, 2005.
- [35] Iven Mareels Paul de Wit Romeo Ortega. “Indirect Field Oriented Control of Induction Motors is Robust Globally Stable”. In: *Proceedings of the 34th Conferece on Decision and Control*. 1995.
- [36] Huei Peng Fengchun Sun Xiaosong Hu Shengbo Li. “Robustness analysis of State-of-Charge estimation methods for two types of Li-ion batteries”. In: *Journal of Power Sources* 217 (2012), pp. 209–219.